Naval Research Laboratory
Washington, DC 20375-5320

NRL/7220/MR—2024/2

The Fate of Aerosol in the Free Troposphere

DR. JULI I. RUBIN

Remote Sensing Physics Branch
Remote Sensing Division

March 26, 2024

DISTRIBUTION STATEMENT A: Approved for public release; distribution is unlimited.

REPORT DOCUMENTATION PAGE

PLEASE DO NOT RETURN YOUR FORM TO THE ABOVE ORGANIZATION

1. REPORT DATE	2. REPORT TYPE	3. DATES COVERED	
		START DATE	END DATE
26-03-2024	NRL Memorandum Report	10-01-2018	12-31-2023

4. TITLE AND SUBTITLE
The Fate of Aerosol in the Free Troposphere

5a. CONTRACT NUMBER	5b. GRANT NUMBER	5c. PROGRAM ELEMENT NUMBER
5d. PROJECT NUMBER	**5e. TASK NUMBER**	**5f. WORK UNIT NUMBER**
		1L26

6. AUTHOR(S)
Dr. Juli I. Rubin

7. PERFORMING ORGANIZATION / AFFILIATION NAME(S) AND ADDRESS(ES)
Naval Research Laboratory
4555 Overlook Ave SW
Washington, DC 20375-5320

8. PERFORMING ORGANIZATION REPORT NUMBER
NRL/7220/MR—2024/2

9. SPONSORING / MONITORING AGENCY NAME(S) AND ADDRESS(ES)	10. SPONSOR / MONITOR'S ACRONYM(S) NUMBER	11. SPONSOR / MONITOR'S REPORT NUMBER(S)
Naval Research Laboratory 4555 Overlook Ave SW Washington, DC 20375-5320	NRL	

12. DISTRIBUTION / AVAILABILITY STATEMENT
DISTRIBUTION STATEMENT A: Approved for public release; distribution is unlimited.

13. SUPPLEMENTAL NOTES

14. ABSTRACT
A major challenge in characterizing the fate of aerosol in the free troposphere is the lack of aerosol observations, with very limited vertical information. The goal of this project is to investigate the use of water vapor as a tracer for free tropospheric aerosol injection and transport through quantification of aerosol and water vapor relationships, the drivers of these relationships, and what they tell us about aerosol life cycle through a combination of model and observational evaluations.

15. SUBJECT TERMS
atmospheric aerosol, water vapor, synoptic transport, free tropsophere

16. SECURITY CLASSIFICATION OF:			17. LIMITATION OF ABSTRACT	18. NUMBER OF PAGES
a. REPORT	b. ABSTRACT	c. THIS PAGE		
U	U	U	SAR	36

19a. NAME OF RESPONSIBLE PERSON	19b. PHONE NUMBER *(Include area code)*
Dr. Juli I. Rubin	(202) 767-2951

This page intentionally left blank.

NRL Technical Memo: The Fate of Aerosol in the Free Troposphere

1. INTRODUCTION

Aerosol particles, including those contained in dust, smoke, sea salt, and pollution, are ubiquitous in the atmosphere. While aerosol loadings tends to be concentrated in or around the boundary layer, injection events can occur in which aerosol is introduced into the free troposphere, often increasing the lifetime and allowing for transport over large distances. These major injections directly impact Navy operations by impeding aviation operations, degrading electro-optical visibility, and contaminating remote sensing signals. There have been extensive studies on the lofting mechanisms for intercontinental free tropospheric aerosol events, such as the injection of ash through volcanic eruptions or the injection of smoke by convection. However, the fate of these particles as plumes are transported and disperse is not well characterized, which is important for modeling efforts as well as for quantifying aerosol radiative impacts. This knowledge gap is a result of limited aerosol observations in the free troposphere, particularly for observing the temporal evolution of aerosol. As a result, free troposphere aerosol transport and impacts are often mischaracterized in Navy aerosol forecasting systems.

A major challenge in characterizing the fate of aerosol in the free troposphere is the lack of aerosol observations, with very limited vertical information. While big injection events can be remotely sensed due to a strong aerosol signal, as the aerosol dissipates, the signal weakens and becomes difficult to observe and quantify. Lidars, while being quite precise, have poor sampling. Passive estimates of plume heights have the opposite, coverage but poor specificity and large errors. A new approach for overcoming the lack of aerosol observations is use other atmospheric constituents as tracers, for example using water vapor measurements to track aerosol transport and ultimatley fate in this under-observed region. While the aerosol and water vapor relationship is generally accounted for in the context of relative humidity, hygroscopicity, and optical properties (e.g., Hänel et al., 1976; Charlson et al. 1992), the covariability of aerosol particles and dispersed water vapor is important in its own right. Early studies of co-located aerosol and water vapor measurements demonstrated the structural covariability between the two components (e.g, Stull and Eloranta 1984; Kleinman and Daum, 1991; Turner 2002; De Tomasi and Perrone, 2003). Now, coupled aerosol-water vapor profiles are commonly used to infer aerosol layer structure (e.g., Livingston et al., 2003; Reid et al., 2003; 2008; 2019), cloud detrainment (Su et al., 2011; Reid et al., 2019) and mixed layer properties (Späth et al., 2016). Additionally, the use of water vapor measurements to support aerosol applications is strengthened by similarities in transport patterns that are regularly observed in both satellite water vapor (e.g., MIMIC-TPW, Wimmers et al. 2011) and aerosol optical depth (AOD) as well as Navy modeling systems (Figures 1 and 2). These simlarities in transport are expected given coherent syntopic flowpatterns that co-transport aerosol and water vapor as part of their life cycles. At the same time, water vapor is a highly observed quantity, much more so than aerosol, with an array of observations available from satellites and soundings. More recently, next generation geostationary satellite sensors also provide an expanded capability. The Advanced Baseline Imager and Advanced Himawari Imager (ABI, AHI), onboard GOES-16 and Himawari-8, provide infrared measurements of water vapor emissions in

Manuscript approved March 25, 2024.

three channels, giving vertical information at unprecedented spatial and temporal resolutions that have a potential use for tracking free tropospheric aerosol events.

In order to understand the application of water vapor observations to free tropospheric aerosol events, the goal of the presented work includes: 1) quantifying the relationship between aerosol and water vapor with a focus on the free troposphere 2) identifying the drivers of these relationships and 3) understanding what water vapor-aerosol covariability tells us about aerosol in the free troposphere in terms of life cycle. The importance of these questions extends beyond developing a better understanding of aerosol life cycle. Findings to these questions can be applied to identify areas of improvement needed in Navy aerosol models. Additionally, the aerosol and water vapor relationship can be utilized in coupled aerosol and meteorological data assimilation in order to improve global aerosol forecasts, especially in the vertical distribution. Finally, the aerosol and water vapor co-transport is relevant for their relative contributions to overall solar and terrestrial radiative effects (Gutleben et al., 2019).

2. APPROACH

The approach used for evaluated the posed questions included a combined analysis of observational datasets and Navy model output with a focus on synoptic-scale aerosol events and their life cycle in the free troposphere. Observational evaluations included a combination of satellite, aircraft, and ground-based observations. Navy aerosol prediction systems are used, including operational output from the Navy Aerosol Analysis Prediction System (opsNAAPS), the NAAPS reanalysis (NAAPS-RA; Lynch et al. 2016), and a new ensemble version of the NAAPS system (ENAAPS; Rubin et al. 2016) which is ideal for looking at model sensitivities. Additionally, meteorological fields from the Navy Global Environment Model (NAVGEM; Hogan et al. 2014) and its ensemble are included. The observational analysis leveraged ongoing collaborations with the NRL Marine Meteorology Division using their in-house processing of ABI/AHI within the Geo-located Information Processing System (GeoIPS), a satellite and model processing system. Radiosondes and a range of aerosol-related satellite, ground, and field observations are also used. Results the from modeling and observational analyses are tied together to first quantify the aerosol and water vapor relationship as described below:

-The globally mapped relationships between AOD and total precipitable water vapor (PW) was evaluated to our knowledge for the first time, at daily to seasonal levels using approximately 20 years of NASA's Aerosol Robotic Network (AERONET; Holben et al., 1998; Giles et al., 2019) and the 16-year NAAPS-RA model fields. The advantage of AERONET for this study is that the data record is long and includes high frequency ground-based measurements of both aerosol in the form of AOD and water vapor in the form of PW with sites located across the globe. Additionally, AERONET measurements are made throughout the entire daylight hours when the sun is not obscured by clouds. AERONET observations, with small associated uncertainties, was combined with the reanalysis fields with global coverage in order to provide a best estimate of the seasonal AOD and PW relationships, including an evaluation of correlations, slope (Theil-Sen Regressions), and PW probability distributions for identification of statistically significant differences in PW for high AOD events. The relationships produced from the AERONET and NAAPS-RA datasets were compared against each other as a means of understanding Navy model performance in capturing these relationships. A more detailed description of this evaluation is included in Rubin et al. (2023).

- While the global and AERONET site/NAAPS-RA AOD and PW evaluations conducted as part of this project, as well as the studies cited in the introduction, provide an understanding of the column-integrated relationship between aerosol and water vapor, an additional evaluation was conducted to look at the aerosol and water vapor relationship in different levels of the troposphere. This evaluation was conducted using the NAAPS-RA fields only, since observations of joint

aerosol and water vapor vertical structure are limited. Model generated correlations were calculated for a defined boundary layer (BL), lower free troposphere (LT), mid-free troposphere (MT), and upper free troposphere (UT) region. The reanalysis total aerosol extinction and specific humidity were vertically integrated in the first 1km of the atmosphere as a representation of the boundary layer. Integration levels in the free troposphere were selected based on the sensitivities of the upper, mid-level, and lower-level geostationary water vapor channels on the NOAA Geostationary Operational Environmental Satellite (GOES) Advanced Baseline Imager (ABI) and the JMA Advanced Himawari Imager (AHI) with a goal of using these water vapor channels to further explore aerosol and water vapor relationships in future work. The selected integration levels were from 800 to 500 hPa (LT), 600 to 300 hPa (MT), and 400 to 300 hPa (UT), respectively. The vertically integrated relationships, as was done for the full column-integrated evaluation, are calculated seasonally and are used to identify if the model correlations are controlled by aerosol and water vapor in certain parts of the atmosphere. While the boundary layer is expected to be a dominant control of the signal, given the sources of both aerosol and water vapor are within the boundary layer, strong correlations within the free troposphere could indicate aerosol and water vapor relationships as a result of lifting from the surface or long-range transport which typically occurs within the free troposphere.

- It is well documented in the literature that hygroscopic water uptake by aerosol particles under moist conditions impacts aerosol optical properties. Because of such hygroscopicity, it is necessary to understand how much AOD and PW relationships are through co transport, and how much through additional covariability of PW and relative humidity. Global data to evaluate this observationally is not available, therefore, the NAAPS-RA is used to evaluate the impact of the hygroscopic growth factor on model predicted correlations. As a first step in this evaluation, the correlation between PW and relative humidity was calculated by season for the previously defined vertical components of the atmosphere (boundary layer, lower/mid/upper free troposphere). In order to calculate relative humidity for each defined part of the troposphere, a saturation specific humidity was calculated in each model level using the reanalysis pressure and temperature fields as input. Both the specific humidity and the saturation specific humidity were vertically integrated over the defined levels and the ratio of the two values was used to produce a relative humidity that conserves the amount of water vapor through the associated portion of the troposphere. This analysis gives a first look at where the covariability between PW and RH is expected to be most impactful on the AOD and PW relationship. However, given aerosol hygroscopic growth is dependent on aerosol type, the analysis was taken a step further by calculating the seasonal relationships, including correlations, slopes (Theil-Sen Regressions) and the probability distribution evaluation, between dry AOD and PW. The dry AOD, in which the impact of hygroscopic growth on AOD is removed as described in Rubin et al. (2023), was calculated for the full dataset. The relationships using the dry AOD are compared to the standard AOD/PW results as a means to evaluate the impact of hygroscopic growth on the modeled AOD and PW relationships.

-The global evaluation performed under this project was used to provide an understanding on regions and seasons for which statistically significant relationships between aerosol and water vapor are present on both observations and models. From this global evaluation, case study evaluations were selected for further investigation based on the strength of the observed/modeled relationships. This included individual events at AERONET sites, including representative pollution, dust, and biomass burning aerosol events at different locations around the globe. Additionally, specific aerosol events were evaluated in detail using satellite-based datasets for tracking both aerosol and water vapor. One such example is the extreme Australian wildfires that occurred in December 2019-January 2020 and circumnavigated the globe as discussed in Kablick et al. 2020. Case study evaluations were also conducted using data from a number of field

campaigns combined with Navy model output. The field campaign studies included measurements taken during the Studies of Emissions, Atmospheric Composition, Clouds and Climate Coupling by Regional Surveys (SEAC4RS; Toon et al. 2016) field campaign in 2013, the Cloud, Aerosol and Monsoon Processes Philippines Experiment (CAMP2Ex; Reid et al. 2023) field campaign in 2019, and the Convective Processes Experiment Aerosols & Winds (CPEX) experiment in 2021 and 2022. The focus of field campaign evaluations was vertical observations from LIDAR instruments combined with soundings. More specifically for the CPEX campaing, the focus was on NASA Langley's High Altitude Lidar Observatory (HALO; Nehrir et al. 2018) which was flown during the mission and provides joint aerosol and water vapor profile measurements.

The results from the above evaluations of aerosol and water vapor relationships were tied together with meteorological information to help identify drivers of such relationships and determine implications for free tropospheric aerosol life cycle as described below:

-In addition to the global AERONET evaluation of AOD and PW relationships, Principle Component Analyses were conducted on AERONET fields to determine if aerosol and water vapor relationships are found on an event-level in space and time and to evaluate what drives the variability in the AOD and PW relationship. The PCA analyses were conducted regionally to account for spatial gaps in the dataset and also to account for potential differences in the driving meteorology by region. Regions of focus had the greatest density of AERONET sites, including the United States and Europe. Ordinary kriging was used to fill in missing data with sensitivity tests conducted on the domain size and krigging parameters. Satellite and model-based meteorological data (NAVGEM) was then combined with the analyses as a means to evaluate meteorological drivers.

-Meteorological information was brought into all of the case study evaluations in order to facilitate the understanding of drivers and life cycle for the synoptic-scale free tropospheric events of interest. For field campaign evaluations, this included NAVGEM fields as well as soundings and satellite data, including the geostationary satellites.

-All evaluations conducted included comparisons of observational and model fields (opsNAAPS, NAAPS-RA, ENAAPS). Identified differences were used to detect missing or incorrectly characterized model processes that require attention in future development efforts for predicting free tropospheric aerosol events.

3. RESULTS

3.1 Global Evaluation of Aerosol and Water Vapor Relationship

As aerosol regimes are typically seasonal in nature, all evaluations are performed for December, January, February (DJF)-March, April, May (MAM)-June, July, August (JJA)-September, October, November (SON). Regressions of AOD and PW for the daily data by season, including correlation coefficients and slopes, and the statistically significant difference in mean PW between the distribution associated with high AOD events only and the full PW distribution for both the NAAPS-RA and AERONET daily data are presented in Figure 3. Red regions/sites indicate a positive correlation in which higher PW is associated with higher AOD values and blue regions indicate a negative relationship in which lower PW is associated with high AOD values. For all evaluations in Figure 3, the predominant signal is positive (ie. red) in both the AERONET observations and the NAAPS-RA with the strongest correlations varying by season, and/or aerosol regime. The NAAPS-RA daily correlations (Figure 3) within seasonal aggregates indicate similar but not identical spatial patterns relative to the AERONET dataset. The dominant positive correlation regions include the Eastern/Southeastern United States as is found in AERONET. Likewise, stronger European AOD and PW correlations are found in the summer months (JJA), in Eastern Asia in the winter

season (DJF), and the Middle East in the fall (SON). The NAAPS-RA results are helpful in that it provides a more complete perspective on the AOD and PW relationships.

Although positive correlations are dominant throughout the world, negative correlations were also identified in both the AERONET and NAAPS-RA datasets from daily data. In the AERONET dataset, negative correlations are limited to the tropic/subtropics with negatively correlated regions mostly associated with biomass burning. During all seasons, negative correlations are found in the Sahel region in both AERONET and the NAAPS-RA with the negative relationships extending further northwards in the boreal spring and summer months. This results in an exceptionally strong dipole between Saharan and Sahelian outflow and is likely related to shifts in the Intertropical Convergence Zone (ITCZ). This points to aerosol sources (biomass burning and dust) and scavenging as a cause of the negative AOD and PW relationship. The NAAPS-RA shows these negative correlations extending into the Atlantic Ocean with seasonally dependent differences. Negative correlations extend into the Caribbean in JJA and to northern parts of South America in MAM, consistent with seasonal transport pathways. Other negative correlation regions include Southeast Asia, South America, and Southern Africa. For these regions, the strongest negative correlations are associated with the respective dry, burning seasons. For example, negative correlations are strongest in Peninsular Southeast Asia in MAM and in Insular Southeast Asia and South America in SON. In these cases, negative AOD and PW relationships are a result of higher aerosol emission occurring under dry conditions, which lead to more fire activity.

The global and seasonal pattern in the positive and negative Theil-Sen slopes are consistent with the correlation analysis results (Figures 3). The biggest Theil-Sen slopes tend to occur where larger interquartile ranges (IQR) ranges in AOD are present. The largest slopes in both datasets are centered on Beijing in the DJF months with values exceeding $1cm^{-1}$. Beijing consistently has some of the largest positive changes in AOD with PW in the AERONET dataset for all seasons with values, including 95% confidence intervals, of 1.1(1.0-1.2), 0.35(0.32-0.38), 0.46(0.43-0.51), and 0.26(0.22-0.3) cm-1 for DJF, MAM, JJA, and SON, respectively. The NAAPS-RA is largely consistent with AERONET for the DJF and MAM months with corresponding values of AOD:PW slopes, 1.13(1.08-1.18), and 0.31(0.29-0.33) cm^{-1}. Less sensitivity to PW is found in the reanalysis for JJA and SON with corresponding values at Beijing of 0.13(.11-0.14), and 0.18 (0.17-0.20) cm-1. This is likely due to an underestimation of haze formation within NAAPS, as with other global models (e.g., Sessions et al., 2015; Xian et al., 2019) and also possibly due to the underestimation of AOD in summer from NAAPS due to a low AOD bias in the assimilated satellite AOD datasets in the East Asia region (Eck et al., 2018). Large positive changes in AOD with PW extend through Asia, the Middle East, and Northern Africa, all regions impacted by high AOD events. As is the case in the correlation results, the strong dipole in slopes is clear over North Africa with positive slopes to the North and negative slopes in the southern Sahel region. Likewise, negative slopes are mainly associated with burning regions.

While the correlation and slope evaluation is used to define a seasonal AOD and PW relationship across the datasets, it is expected that variations in the aerosol and water vapor relationship will exist across air masses. As a result, a probability distribution evaluation is another useful way to examine the data. The seasonal evaluation of the probability distributions is included in Figure 3, next to the correlation and slope results. The plots show the statistically significant difference in the mean for the PW distribution associated with high AOD events (AOD values more than 1 standard deviation above the mean) and the full PW distribution. Red regions/sites indicate that the PW mean for high AOD events is statistically higher than the full distribution mean (i.e. higher moisture levels). Blue regions/sites indicate a lower PW mean for high AOD events (i.e. dryer conditions). Regions or sites in white have no statistically significant difference. The spatial pattern in the probability distribution evaluation are similar to the correlation and slope analysis, however, the probability distribution evaluation highlights different regions than the previous analyses. For example, across all seasons, larger changes in PW for high AOD events are observed in Argentina, South America. This is a region that is impacted by both local pollution and transported

biomass burning (Resquin et al. 2018). Larger changes in PW for high AOD events are also observed over Northern Australia during MAM, which is consistent with peak bushfire season in the region. Larger changes in PW are also found over the United States and Canada, consistent with patterns in the correlation evaluation, but with more pronounced values relative to other locations. ABF is generally the dominant aerosol type with biomass burning from Central America and Western US/Boreal Regions during the MAM and JJA seasons, respectively. Likewise, Eurasian Boreal regions associated with biomass burning activity during JJA are more pronounced in the PW distribution evaluation. The peak in values in the Southeast United States are found during the DJF season. During MAM and SON, the peak areas include most of the Eastern United States and extending into Canada and Central America. However, regions that were more pronounced in the correlation and slope evaluation, have smaller differences in mean PW for high AOD events, Beijing being a good example of this. This is because the probability distribution evaluation is taking into account those infrequent, outlier events that don't affect the Theil-Sen slopes. Locations where the IQR is relatively small, such as the United States, Europe, Australia, and parts of South America and Southern Africa have greater differences in mean PW, despite having small Theil-Sen slopes, due to the impact of outlier events. For many of these regions, the outliers are associated with biomass burning, indicating that PW is a useful tracer for such events.

While the global plots of AERONET and NAAPS-RA AOD and PW relationships give a sense of spatial agreement, a scatterplot comparison of the quantitative values generated from the two datasets are used to take a closer look at the consistency between the observed and predicted relationships. A seasonal comparison of AERONET and NAAPS-RA regressions is shown as a scatterplot in Figure 4, including site by site a) correlations; b) Theil-Sen slopes; and c) the PW mean difference for high AOD events. In addition to the three scatterplot comparisons, all locations for which for the sign of the AOD and PW relationships differed between the AERONET and the NAAPS-RA datasets were identified. For these identified sites, the distribution of AERONET correlations are plotted by season in Figure 4d. This is included as a means to examine the strength of the observed AOD/PW relationship under conditions when the datasets disagree. Overall, the observations and model are in general agreement in the sign of the correlations, slope, and PW difference for high AOD events (Figure 4a-c). Differences in the relationship sign generated by AERONET and the NAAPS-RA occur for sites in which the AERONET-generated correlations are weak, mostly falling below 0.20 (Figure 4d). For the strongest correlation sites, AERONET and NAAPS are in good agreement in DJF and MAM. For JJA and SON, NAAPS-RA has a tendency to produce weaker relationships relative to AERONET. Some differences are expected given that the event sampling is different between the AERONET observations and the 16-year NAAPS-RA. However, the overall agreement between the two datasets provides some confidence in the NAAPS-RA for generating regionally and seasonally varying AOD and PW relationships on a global scale. More detailed results of this evaluation can be found in Rubin et al. 2023.

3.2 Vertical Evaluation of the Aerosol and Water Vapor Relationship

In addition to calculating the full column-integrated AOD and PW correlations in the NAAPS-RA, the correlations were also evaluated by vertically integrating the extinction and specific humidity through previously defined pressure levels in the atmosphere that correspond to the boundary layer, as well as lower, middle, and upper free troposphere that loosley correspond to ABI and AHI 7.34, 6.95, and 6.19 μm water vapor channels. This evaluation was conducted seasonally, like the fully integrated analysis, with results shown in Figure 5. In addition to the global plots, histograms of the AOD and PW correlations for the full column and the vertical components of the atmosphere are shown in Figure 6. It is notable that stronger positive correlations exist when looking at limited parts of the atmosphere compared to the fully integrated column; most evident in the global plots for ocean regions, particularly in the Southern Hemisphere, where correlations exceeding 0.5 occur compared to the fully integrated correlations that are on the order of 0.2. This result is not unexpected given that the vertical components of the atmosphere look

different depending on things like vertical mixing, a local aerosol and water vapor source compared to a long-range transport event, the relative humidity profile etc. Additionally, some regions exhibit stronger correlations in certain portions of the atmosphere. For example, dust dominated regions such as the Sahara, Arabian Peninsula and the Gobi and Taklimakan deserts have the strongest correlations in the middle free troposhere (FT). This level is higher up in the atmosphere than expected, given for example, studies have shown East Asian dust heights to range from 1.9 to 3.1km (Liu et al. 2019) and the typical description of the Saharan Air Layer (SAL) includes dust-laden air between approximately 850 and 500 hPa (Karyampudi et al. 1999) with several other studies identifying Saharan dust up to ~5km for summertime dust transport (Mortier et al. 2016, Veselovskii et al. 2016, Tesche et al. 2011). This indicates that the model may be transporting too much dust aerosol and water vapor higher into the atmosphere and this transport is well correlated. Correlations over North America and Eastern Europe are strongest in the BL to lower FT. Wintertime correlations over East Asia/Beijing are pretty consistent throughout the column. Negative correlation regions associated with biomass burning smoke aerosol, including the Sahel, Southern Africa, and Southeast Asia have the strongest correlations in the lower FT and largely disappear beyond this point. The shift in correlations with vertical location are also evident in the histograms (Figure 6) when compared to the full column distribution. This is particularly the case for the lower and mid free troposphere where the number of grids with correlations greater than 0.5 increase. Additionally, the shift of the correlations to mostly positive can be seen in the mid and upper free troposphere histograms. More detailed results from this evaluation can be found in Rubin et al. 2023.

An important goal of this work was to leverage the geostationary water vapor channels for tracking these synoptic scale aerosol events in which water vapor co-transport occurs. The conducted vertical evaluation is important for assessing which water vapor channels are expected to be most relevant for tracking such aerosol events. For example, based on the analysis, the 6.95um water vapor channel is expected to be the best for tracking large scale dust events while the 7.34 um channel was found to be the most relevant for biomass burning events. Case study evaluations were conducted to see if this is consistent on an event level. For example, evaluations of California wildfire events clearly show cooler brightness temperatures in the 7.34um water vapor channels associated with elevated smoke transport, providing supporting evidence for the vertical analysis (Figure 7) . For dust events, Asian dust cases were evaluated using the Himawari water vapor channels. In this case, the lower level water vapor channels (7.34um) appear to be more informative than the mid-level channel (6.95um). This provides additional evidence that the model is transporting too much dust aerosol and water vapor higher into the atmosphere. The vertical model analysis also indicated that the upper level 6.19um channel is generally not relevant for tracking aerosol events, however, due to injection height representation in the model, these upper levels events are generally modeled as being lower in the atmosphere. This finding was further supported by case study evaluations which show the upper level water vapor channel to be useful for extreme aerosol events. An example of this is the extreme Australian wildfires that occurred during December 2019-January 2020 (Kablick et al. 2020), where signals consistent with aerosol transport are present in the upper level channel. Additionally, events like the Fukutoku-Okanoba volcanic eruption in Japan in 2021 and the Tonga eruption in January 2022 can also be seen in the upper level channel. This evaluation highlights that aerosol vertical distribution is an important area of improvement for Navy aerosol modeling systems and the geostationary water vapor channels can be leveraged for this work.

3.3 Impact of Hygroscopic Growth of Aerosol and Water Vapor Relationships

While relationships between AOD and PW have been demonstrated, this signal can be either from co-transport or a confounding relationship between enhanced PW and RH. The correlation between RH and PW is shown in Figure 8 by season and for the boundary layer and parts of the free troposphere. The largest spatial variations in the PW and RH correlation occur in the boundary layer, as anticipated, with strong correlations found over Africa, extending into the Indian Ocean/India, located further North during JJA and

further South during DJF and similar patterns during MAM and SON. Other regions of high correlation in the boundary layer include off the coast of South America, parts of Australia, and limited locations in the tropical oceans. Beyond the boundary layer, the overall patterns are generally consistent throughout the vertical column with strong correlations in the subtropics and tropics (>0.9) with some variations on the extent by season. In this highly correlated region, hygroscopic growth is expected to be a significant driver in AOD and PW relationships when dust is not the dominant aerosol type. RH and PW correlations are higher over ocean regions than over land in the northern hemisphere, which should be impactful for sea salt aerosol and PW correlations.

The impact of the RH and PW correlations on the AOD and PW relationship are shown in calculated seasonal relationships between "dry" AOD, which excludes the impact of hygroscopic growth, and PW in the NAAPS-RA in Figure 9. This figure includes the correlations, the slope of the "dry" AOD and PW relationship, and the statistically significant different in mean PW for high "dry" AOD events. The removal of hygroscopic growth from the AOD calculation had the following outcomes on the resulting correlations: 1) the previously positive correlation found was reduced in magnitude 2) the previously negative correlation coefficient became more negative 3) the sign of the correlation flipped from positive to negative and 4) little to no change in the correlation. Regions such as the Eastern United States and Europe fall into the first category where positive AOD and PW correlations are found for all seasons, but the correlation coefficient is greatly reduced. For the Eastern United States, peak correlation coefficients were in the approximately 0.6-0.7 range with hygroscopic growth and fell below 0.5 without it. Likewise, positive correlations in Europe are still present, but weakened. In these cases, hygroscopic growth amplifies an existing positive relationship that is somewhat weak when evaluating seasonal data by correlation. In regards to the second category, this corresponds to regions dominated by smoke aerosol that previously exhibited negative AOD and PW relationships, such as Peninsular Southeast Asia during the MAM months and Insular Southeast Asia during the SON months. Additionally, increases in negative correlations are found for aerosol transport from Asia across the Pacific Ocean. In these cases, hygroscopic growth reduces an existing negative relationship between aerosol and water vapor. Ocean regions mostly account for the third category where the correlation flipped from a weak positive to negative value. Regions that are dominated by dust, including the Sahara and Arabian Peninsula, fell into the fourth category as there is no hygroscopic growth for dust in NAAPS. More detailed results from this evaluation can be found in Rubin et al. 2023.

3.4 AERONET Case Study Evaluations of the Aerosol and Water Vapor Relationships

In order to further understand regional differences in observed AOD and PW relationships identified in the global evaluations, individual sites in which strong AOD and PW relationships were identified and had several years of observational data available were selected for further analysis. Selected sites included the Tallahassee, Florida site for Southeast US pollution; Beijing, China for Asian haze and dust; Izana, Canary Islands for Saharan dust; and Alta Floresta, Brazil for South American biomass burning. All selected sites exhibited a positive AOD and PW relationships with the exception of the Alta Floresta site, which had negative relationships in the global evaluation. Observational and model timeseries were analysed for these selected sites in order to provide a more detailed understanding of the relationships on an event level. Example time series evaluations are shown in Figures 10 and 11 for the Tallahassee and Izana sites, respectively.

At the Tallahassee site, the predominant aerosol type is anthropogenic and biogenic fine/pollution and although AOD values are generally low during DJF, strong AOD and PW relationships were found with correlations of 0.74 in the AERONET dataset and 0.66 in the NAAPS-RA with PW mean differences around 1cm for high AOD events. The daily-averaged AOD and PW timeseries for the 2018-2019 DJF season are shown in Figure 10a. The timeseries indicates, consistent with the correlation analysis, that the daily-average AOD and PW generally move together. There are several joint peaks in AOD and PW that occur during the time period and three selected cases are examined further, including 1/1/2019, 2/7/2019,

and 2/17/2019, with these events identified in the Figure 10a timeseries using red arrows. The AERONET AOD and PW timeseries for these three cases are shown in Figures 10b-d, respectively. The timeseries show the AOD and PW are generally consistent through the day, indicating that the AOD and PW relationships can extend to sub-daily timescales. For all evaluated cases at Tallahassee, coincident transport of AOD and PW is observed in the reanalysis fields, associated with a frontal system.

Data is also examined at the Izana, Canary Island site in Figure 11. The Izana site, which is located approximately 300km west of the African coast, is particularly useful for evaluating aerosol and water vapor relationships for free tropospheric dust. It has also been noted in the community that against a Saharan air layer free subsidence regime, the infrared signals of Saharan Air Layer dust are quite small relative to co-transported water vapor (Gutleben et al., 2019; Ryder, 2021: Barreto et al., 2022). Nevertheless, forecasters have found the water vapor signal useful in tracking dust events (Kuciauskas et al., 2018). Izana is a mountain site located at approximately 2400m, above a strong subtropical temperature inversion layer which makes it ideal for monitoring free tropospheric plumes. In the summer months, frequent and intense Saharan air mass outbreaks in the subtropical free troposphere impact the site. Particularly large AOD dust storms were observed transporting Saharan dust across the Atlantic in the summer of 2020, including the so called "Godzilla" dust event in June that has been examined in detail in previous studies (Francis et al. 2020). As a result, this time period was evaluated in further detail at Izana with a focus on several dust events. In the analysis conducted in this work, positive relationships between AOD and PW were found in both the AERONET and NAAPS datasets at Izana during the JJA season with the AERONET dataset having a correlation of 0.66 and the NAAPS-RA indicating a weaker correlation of 0.48. This difference may be due to altitude effects at the Izana site which may not be captured in NAAPS. The daily-average AOD and PW timeseries for the 2020 JJA season at Izana are shown in Figure 11a. The AOD and PW are moderately-well correlated, although there are PW peaks present without the presence of aerosol. As sources of aerosol and water vapor are different, this is not unexpected. Three of the peak from the timeseries as indicated by the red arrows were selected for further evaluation, including 6/14/20, 7/18/20, and 7/31/20 with timeseries shown in Figures 11b-d, respectively. As was shown for the previous pollution cases, the AOD and PW are well correlated in the non-averaged dataset showing the presence of correlations for dust events on timescales less than a day. The NAAPS-RA AOD and PW fields are shown for the 6/14/20 case in addition to the associated dropoff of both AOD and PW on 6/18/20, as well as for the 7/18/20 and 7/31/20 events in Figure 11e. For the 6/14/20 case, CALIPSO indicates dust tops near Izana at around 5km. A cutoff low was present to the northwest of Africa and a subtropical high over the Western coast of Africa which resulted in increased dust generation and recirculation. The southwesterly winds transport the dust to Izana on June 14 and at the same time, moist ocean air shown by the PW fields is transported to Izana as well, resulting in a spike in both AOD and PW at the AERONET site. On June 18, the moisture and dust begin pushing south and west across the Atlantic, resulting in decreases in AOD and PW at the same time at Izana. Similar examples of dust and water vapor cotransport are shown for the 7/18/20 and 7/31/20 cases. These results are consistent with previous studies which have indicated enhanced water vapor mixing ratios associated with the dust in Saharan Air Layer events (Marsham et al. 2008, Jung et al. 2013, Kanitz et al. 2014). Thus, Izana is a good example of subtropical free tropospheric co-transport of water vapor and dust.

Additional sites examined include Beijing, China and Alta Floresta, Brazil (Rubin et al. 2023). In Beijing and China in general, the monsoon was identified as an important control in the aerosol and water vapor relationship, which determines the direction/intensity of atmospheric flow and the amount of water vapor/precipitation. At the Beijing site for example, pollution cases were found of weakened monsoon flows during wintertime (when strong correlations were identified) leading to stagnant conditions, resulting in build-up of both aerosol and water vapor followed by co-transport with the eventual movement of the air mass out of the region. At Alta Floresta, while the overall seasonal signal was found to be negative, on an event level the relationship between aerosol and water vapour was found to be positive when associated with transport. On the other hand, drier conditions were identified when local fires were impacting the

region. When examining the timeseries at Alta Floresta in the SON season when the correlations were found to be the strongest, a clear downward shift in the PW fields occurs during October, consistent with monthly site climatologies from AERONET (3.61cm in September, 4.15cm in October, 4.5cm in November). As fires are associated with dry conditions, the AOD fields decrease as the water vapor increases. This shift towards wetter and decreased aerosol conditions is driving the seasonal negative correlations for biomass burning regions. However, despite this overall shift, peaks in AOD and PW were found to be positively related at this site for transported aerosol at the event level.

3.5 AERONET Principle Component Analysis

In order to further understand the relationships found in the global correlation analysis, a principle component analysis (PCA) was conducted on the AERONET data to evaluate the temporal and spatial correlations and understand the sources of variability. PCA is a data reduction technique that is used to transform correlated variables into orthogonal, linearly uncorrelated principle components (PCs).The PCA analyses were conducted regionally since differences in types of aerosol events and meteorology may be present. An important aspect of this analysis is generating the data used as input for the PCA. A dataset was created that includes the site and associated variable, either AOD or PW, as the data columns. The rows of the dataset are the measurements in time. However in PCA, a complete dataset without missing data is needed. As this is not the case for combined site data where measurements at each site are made independently, a method for filling in the dataset was necessary. As a first step, the sites were screened such that they had to have 70% of the complete data record, leaving the longest running and most consistent sites. The next step was to fill in any missing data, which was done with Ordinary Kriging (OK). For any missing data value, the nearby data points (all sites) are weighted based on their distance to the point of interest, applying a variogram to describe how the relationship is expected to change with distance. The range of the variogram is the distance at which the points are not expected to have a relationship. A correlation lengthscale analysis was conducted as a means to define the range of the variogram for kriging of AOD and PW. The seasonal correlation lengthscale evaluation conducted for the Eastern United States is shown in Figure 12 with the same analysis conducted for Europe with the PW correlation lengthscale being longer than the AOD lengthscale. All available AERONET data for a given day are used in the OK with the krigging applied to the site data to generate a 2-d field of either AOD or PW. Krigged datasets were generated with different criteria, including 5, 10, or 15 data points needed for krigging to occur, otherwise, the data row was dropped. The 15 data point criteria is the strictest, resulting in the least number of rows in the dataset (Table 1). The resulting datasets were then run through PCA.

From the PCA analysis, the percent of variance explained is shown in Table 1, the timeseries of the first four principle components is shown in Figure 13 and some additional regionally-specific results are shown in Figures 14 and 15 for Eastern United States and Europe respectively. The first PC explained more of the variance in the Eastern US domain with approximately 60% explained while Europe was around 40%. The first PC had a strong seasonality for both regions with peaks generally occurring in summer months and a positive relationship between AOD and PW. The second PC for both regions had a negative relationships between AOD and PW. Examination of high PC1 value events in both the Eastern United States and Europe domains had both high AOD and PW values associated with them and via inspection by satellite data, were found to be associated with synoptic-scale transport of biomass burning aerosol and also dust aerosol transport from the Sahara towards Europe. These large-scale transport events are associated with frontal transport and extratropical cyclones, explaining the largest amount of the variability for these regions between aerosol and water vapor in their column-integrated forms. The second PC, which explained approximately 12% of the variance in the Eastern United States domain and a slightly higher percent in Europe, exhibited a negative relationship between aerosol and water vapour. Inspection of satellite data associated with high PC2 values regularly showed widespread fires that were local to the domain. These events appear to occur under dry conditions, with little cloud cover, and the smoke isn't transported into

the domain via pathways associated with PC1. On the opposite end, large-scale cloud cover with clean aerosol conditions are also associated with PC2. The remaining PCs appear to be associated with positional shifts in aerosol and water vapor transport events, projecting onto some of the sites and not others. For example, smoke events are observed that impact northeastern AERONET sites, but not the rest of the domain. These positional shifts account for most of the remainder of the variance in the dataset. These results support some of the AERONET case study evaluations conducted and help to link meteorological drivers to the relationships found in the global evaluation.

3.6 Australian Wildfire Evaluation

The 2019-2020 Australian wildfire season was quite extreme with uncontrolled bushfires associated with a severe heat wave and strong surface winds that worsened fire conditions. A number of pyrocumulonimbus (pyroCb) events were identified during this time period with smoke injection as high as 16km (Kablick et al. 2020) with estimates of aerosol mass injection between 0.3–0.9 Tg (Peterson et al., 2021). The injected plumes were tracked in space and time using a combination of Cloud-Aerosol LIdar with Orthogonal Polarization (CALIOP; Winker et al., 2010) for aerosol extinction, Microwave Limb Sounder (MLS) for water vapour mixing ratios, and ultraviolet aerosol index (UVAI) values retrieved from the Ozone Mapping and Profiler Suite (OMPS) with high values indicating the presence of elevated absorbing aerosol such as from smoke. Several plumes were tracked, including one that circumnavigated the globe. Co-transport of the smoke aerosol and water vapor are observed in the plume as it rises and is transported in the lower stratosphere. With this smoke event was an unprecedented amount of water with MLS observations exceeding 15 ppmv with enhanced water vapour detected over 1.5 months after the original event, allowing for extended plume tracking. Detailed results from this evaluation are included in Kablick et al. 2020. This event demonstrates the utility of water vapor as a tracer for these large scale aerosol events and is expected to apply to other upper troposphere/lower stratosphere events such as volcanic aerosol which can be seen in the upper level water vapor channels from the geostationary satellites.

In addition to evaluation of this event through observations, Navy aerosol model performance was also evaluated. In terms of AOD evaluations, the models do predict the smoke events, however, AOD values are biased low and some regions of high AOD that can be seen in the MODIS true color images are missing in the Navy models (Figure 16). While AOD evaluation is useful, it only tells us about the full column. A vertical evaluation of the model aerosol and water vapor was conducted through integration of aerosol extinction and specific humidity over defined vertical ranges (Figure 16). The results from this evaluation show that the majority of the aerosol near the source region is contained within the 400m to 2km range. This is much lower than the extreme injection heights observed for the smoke in the observational analysis described Kablick et al. 2020. This smoke case study as well as additional smoke events (summertime smoke in the United States) that were evaluated through the models and observations such as lidar, consistently showed that the models have issues with smoke injection heights. This leads to issues in forecasted smoke, as the height of injection will impact the transport pathways as well as removal processes that impact aerosol lifetime. For example, the Australian smoke is removed much more quickly due to its location in the atmospheric boundary layer than observed with satellite tracking.

3.7 Field Campaign Evaluations

A number of cases were evaluated using a combination of model and field measurements. The global analyses and previously presented case study evaluations indicate that water vapor is a particularly good tracer for smoke and dust aerosol. As such, presented aerosol case studies focus on these large scale transport events. An example of smoke transport is shown over the United States during the SEAC^{4}RS field campaign shown in Figure 17. Satellite fire detection data indicates the presence of a number of fires in California, Idaho and Wyoming with smoke transport along the Rocky Mountains towards Colorado where airborne flights were conducted. The High Spectral Resolution Lidar (HSRL) data indicates the

presence of a number of aerosol layers with moisture associated in particular with the 5km aerosol layer. While the Navy's NAAPS model does indicate the presence of a smoke aerosol layer around 2km, it is missing the distinct 5km aerosol feature. HSYPLIT back trajectories were conducted on the individual observed layers in the lidar data. This evaluation indicates that the layers originate from different locations, with the 5km smoke layer originating from fires in California and the 2km layer coming from Idaho where fires are also observed. The 3.6km layer also passes through Idaho, but at a slightly higher altitude. It is clear from the back trajectories that the aerosol and water vapor tell us something about source region and the smoke injection height. In terms of NAAPS, the aerosol layer at 5km that is missing is again related to issues with aerosol source injection into the atmosphere and how that is represented in the model. The model injects smoke into the boundary layer whereas we can see that the California smoke is injected to 5km. However, of note is that while the model is dry biased, it does contain water vapor at the 5km altitude where aerosol should be present. This indicates that water vapor information can be used to improve aerosol injection representation and transport and enable the models to better capture these types of free tropospheric aerosol events. In addition to smoke events evaluated during SEAC^{4}RS, smoke events were evaluated during the CAMP^{2}Ex campaign. However, these smoke events were generally contained within the boundary layer, so are less relevant for free tropospheric aerosol transport. Despite this, a few points of interest were identified in this analysis. Co-transport patterns were found in AOD and PW, consistent with the global evaluation, for smoke events sampled during the campaign. The Navy model extinction profiles were very consistent with HSRL data, showing that Navy models are better able to capture vertical distributions of smoke that are contained within the boundary layer. Additionally, while the model was found to be dry biased in this region relative to soundings, the hygroscopicity of smoke aerosol was found to be overestimated in the maritime continent. This is relevant, as indicated by the global evaluation, since hygroscopic growth is an important factor in the aerosol and water vapor relationship and would result in an overestimation of the modelled aerosol and water vapor relationship in this region.

Dust was also identified as another aerosol type for which water vapor is a good tracer in the global evaluation. Several dust events were sampled during the CPEX field campaign in the Atlantic, off the coast of Africa. A nice advantage of the CPEX campaign is the inclusion of NASA's High Altitude LiDAR Observatory (HALO) which makes joint measurements of aerosol and water vapor profiles, making it ideal for this project. One such dust event that was sampled during the campaign occurred on September 9, 2022 with a combination of satellite, airborne and model data shown for the event in Figure 18. In Figure 18a, the EUMETSAT dust RGB product is shown with dust indicated by a pink color. The aircraft flight track is shown in red and NAAPS AOD contours are on top. For this event, peak optical depths in the plume were around 0.6 from MODIS. NAVGEM total precipitable water fields as well as surface winds barbs are shown in Figure 18b. Curtains of water vapor mixing ratio with an overlay of winds and aerosol backscatter from HALO are shown in Figures 18c and d, respectively. From the HALO data, a range of aerosol conditions are observed, including dust contained in the marine boundary layer, dust aloft with moisture co-transport, and light dust aloft with clean and dry air below associated with subsidence. The vertical measurements highlight the complexity of conditions observed in the troposphere for Saharan dust. The Navy models, shown for 22˚N and 20˚W which is coincident with the elevated and moist dust layer, are able to represent the dust around 2km with the associated moisture as shown in Figure 18e. In this case, dust aerosol is being lifted in a manner that is commonly associated with the Saharan Air Layer (SAL) in which the hot dust-laden air is lifted over the cool and moist marine boundary layer as it moves westward. Moisture is lifted in this case along with the dust. HYSPLIT back trajectories were run at different altitudes and at different latitudes along the flight track, indicating directional shear with aerosol layers coming from different locations and as a result, having different aerosol and water vapor properties as seen in HALO.

A second, much larger, dust event was sampled during CPEX-CV on September 22, 2022 with peak optical depths from MODIS exceeding 2 for this event (Figure 19). The airborne dust is much more evident in the EUMETSAT product, shown in pink, with NAAPS doing a good job at getting the peak dust in approximately the correct location and altitude, although biased low (Figure 19a,d). As a result of the high

extinction, the lidar signal becomes attenuated with no return from below the dust aerosol layer at around 3km, seen in the HALO curtain data. For this event, the dust aerosol has a negative relationship, with dryer air associated with the dust. The dry air layer can also be seen in the dropsondes (arrow in 18f) within the dust event (-21.23, 14.60) compared to the second dropsonde profile (-19.56, 10.73) outside of the disturbance. In this case, the mechanism is different for dust generation compared to the September 9 case. Here dust with dry air is associated with an easterly wave which turns into a low pressure system. Instead of a positive relationship, the air associated with the dust is dryer than the surrounding air due to the subsidence of the dusty air around the low. These two cases highlight that dust aerosol and water vapor relationships are present, however, it is dependent on the mechanism of dust generation as well as source region.

4. CONCLUSIONS

This project aimed to quantify the aerosol and water vapor relationship for free tropospheric aerosol events, determine the drivers of these relationships and understand what this tells us about free tropospheric aerosol life cycle. The work outlined in this technical memo all points to the conclusion that aerosol and water vapor relationships are prevalent and significant around the globe with positive relationships being dominant, particularly in the free troposphere. These relationships are tied together through meteorological drivers of synoptic-scale transport and can be used to track aerosol events and quantify atmospheric lifetime. The major conclusions of this work are outlined below:

1. Seasonal relationships between AOD and PW are present across the globe at both seasonal and daily levels. Most often AOD and PW relationships are strongly positive at seasonal to daily time scales, especially for species such as pollution and dust. Biomass burning, however, has negative seasonal relationships due to fire proclivity in dry seasons. Nevertheless, positive daily relationships are observed, associated with synoptic-scale transport. For regions like the Sahel, negative relationships between AOD and PW were found with spatial patterns consistent with shifts in the ITCZ in which convection leads to aerosol scavenging.
2. Mid-latitude relationships between AOD and PW appear to be driven by frontal activity. While tropical/subtropical relationships are driven by seasonal monsoon activity, ITCZ, and dry season patterns. Dust transport associated with African easterly waves and cyclones are the link between aerosol and water vapor for the Sahara.
3. The observed correlations between the AOD and PW were stronger when evaluated by vertical level with the strongest correlations identified in the free troposphere, consistent with large scale aerosol and water vapor transport. The location of the strongest correlations varied by aerosol type with dust dominated regions having the strongest correlations in the mid free troposphere and smoke dominated regions having the strongest correlations in the lower free troposphere. Evaluations of dust events with geostationary water vapour channels indicate dust signals in the lower level water vapour channel as opposed to the mid-level channel. This may be indicative of model transport of dust, and any associated water vapour, higher into the atmosphere than should occur. Signals of smoke transport can also be seen in the lower level geostationary water vapour channels, consistent with the global evaluation.
4. Hygroscopic growth of aerosol particles, which is associated with increased relative humidity and often occurs with increasing PW, has a large influence on the observed covariability between AOD and PW, particularly in the mid-latitudes and for non-dust aerosol species. While transport covariance between AOD and PW is present, the imbedded RH to PW relationship is the dominant term. This indicates that PW is a good tracer for AOD, but not necessarily aerosol mass. This finding has relevance for data assimilation applications.
5. Covariability between AOD and PW for dust-dominated events is statistically significant and hygroscopic growth is not an important factor in the model analysis. We are continuing to evaluate

this point through new dust observations out of Barbados, associated with the MAGPIE field campaign.

6. Case study evaluations highlight that the relationship between column-integrated AOD and PW extends into the vertical. This was demonstrated through observational evaluation of the Australian wildfires in which co-transport of aerosol and water vapour was found and used to show long lifetimes of water vapor and smoke on the order of months in the stratosphere. Stratospheric aerosol events are a more straightforward way to demonstrate the co-transport between aerosol and water vapor as there are no sources of either in that part of the atmosphere apart from the injection. This analysis indicates that water vapor is an excellent tracer for these types of stratospheric events, including volcanic eruptions which can be seen in upper-level geostationary water vapour channels. Navy models do not currently simulate these high altitude injection events, but the analysis indicates that water vapor observations can be used to improve smoke injection height representation and volcanoes if added to the modeling system. The troposphere is more complicated to disentangle as observed during SEAC^{4}RS, CAMP^{2}Ex, and CPEX-CV field missions.
7. The vertical case study evaluations in addition to the global probability distribution evaluation, highlights that the story of a given air mass will determine the aerosol and water vapor relationship. So while there is no uniform description of aerosol and water vapour relationship during synoptic-scale transport, the moisture information of an airmass can be used to determine where the airmass came from (confirmed through HYSPLIT back trajectories) and track it as it moves (LIDAR and satellite event tracking), as well as separate it from other aerosol-infused air masses which have different water vapour characteristics (mixing ratio, relative humidity) as demonstrated in the HALO data.

The aerosol and water vapor relationship was quantified, starting from a global perspective and drilling down to regional and then events levels through a combination of observational and model analyses. Case study evaluations for both smoke and dust aerosol based on satellite, field campaign and model data highlight this relationship from a 3-dimensional perspective and the variation of the relationship across air masses due to differences in transport pathways and process differences. This project lays the foundation for understanding the aerosol and water vapor relationship which can be exploited through follow-on work to improve Navy aerosol forecasting of free tropospheric events through issues identified in this work, particularly smoke aerosol injection height, as well as by taking advantage of water vapour observations for aerosol data assimilation. Finally, steps are being taken to quantify the radiative impact of co-located aerosol and water vapor.

Tables

Table 1. Percent of variance explained for the different configurations run through PCA. ECONUS domain size results were pretty consistent, so only the large domain is shown with variations in the krigging criteria. Both the large and smaller domain for Europe are shown.

	ECONUS			Europe (Larger Domain)			Europe (Smaller Domain)		
	Variance Explained (%)			Variance Explained (%)			Variance Explained (%)		
PC	**5**	**10**	**15**	**5**	**10**	**15**	**5**	**10**	**15**
1	63.2	61.3	63.1	42.8	36.9	35.8	40.4	38.7	36.4
2	12.7	12.7	9.0	17.7	13.9	13.1	16.0	14.8	13.3
3	4.9	4.8	4.8	6.6	6.8	6.6	9.8	9.9	10.2
4	3.4	3.5	3.7	5.6	5.5	5.5	7.3	7.3	6.9
5	2.0	2.1	2.4	2.7	3.3	3.2	3.3	3.4	3.4
6	1.8	1.9	2.0	2.3	2.8	2.9	2.8	2.8	3.0
7	1.5	1.6	1.6	1.8	2.5	2.5	2.2	2.3	2.4
8	1.3	1.4	1.6	1.6	2.2	2.1	1.8	2.0	2.2
Total Variance Explained	90.8	89.4	88.2	81.0	73.8	71.7	83.5	81.2	77.9
Total Data Rows	6706	4058	2023	7188	5936	5016	6003	4648	3255

FIGURES

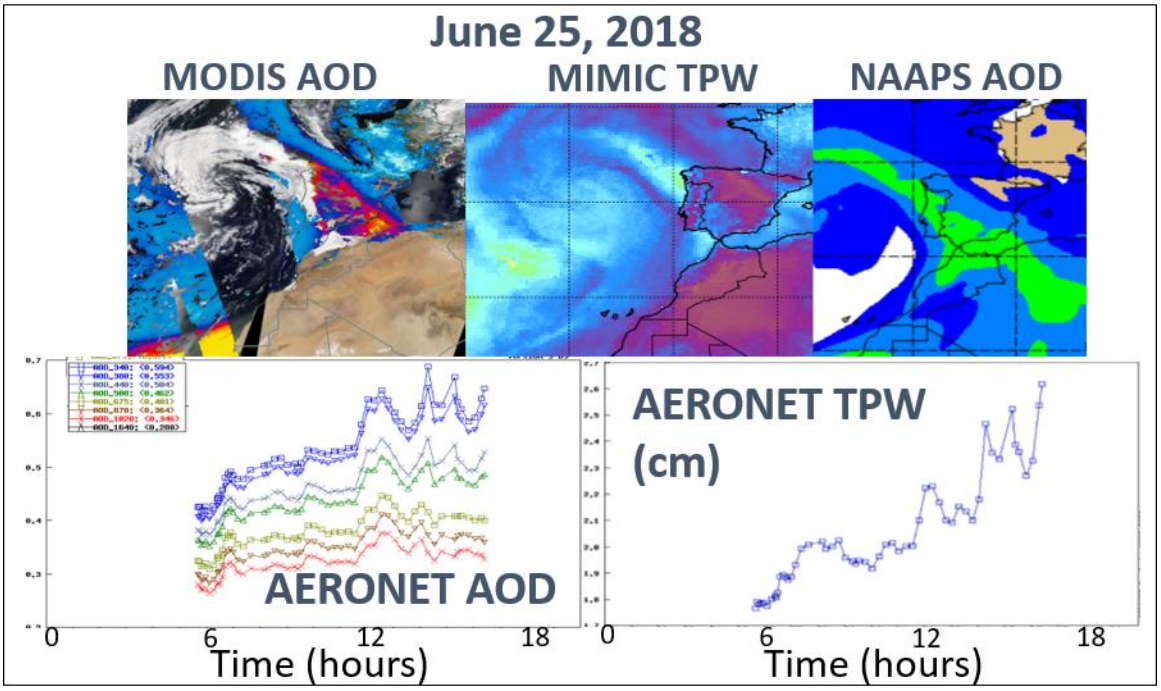

Figure 1. Example observed dust aerosol and water vapor co-transport event on June 25, 2018 moving off of Africa northwards. Both satellite and model-based AOD is shown from MODIS and NAAPS, respectively with total precipitable water shown with the MIMIC TPW satellite product. Additionally, timeseries of AOD and TPW are shown at an impacted AERONET site.

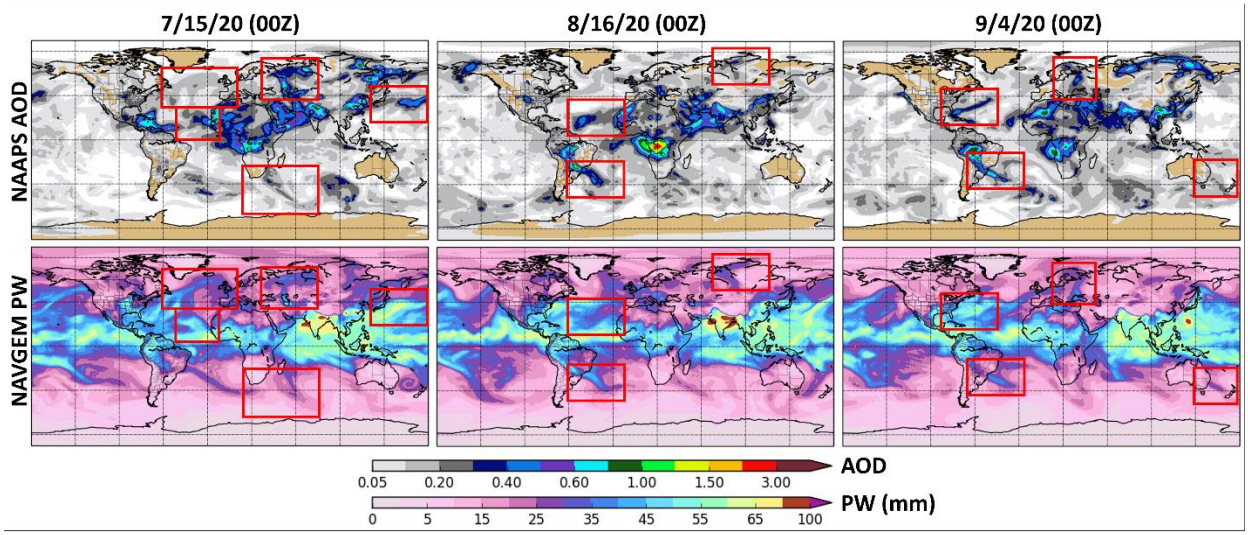

Figure 2. Examples of aerosol optical depth (AOD) and total precipitable water (PW) forecasts from the Navy Aerosol Analysis Prediction System (NAAPS) and the Navy Global Environment Model (NAVGEM), in which similar synoptic scale transport patterns are found, particularly in the mid-latitudes. Aerosol and water vapor features with similar transport patterns are highlighted in matching red boxes in

the AOD and PW plots. These types of co-transport events of both positive and negative correlations are found in forecasts on a daily basis.

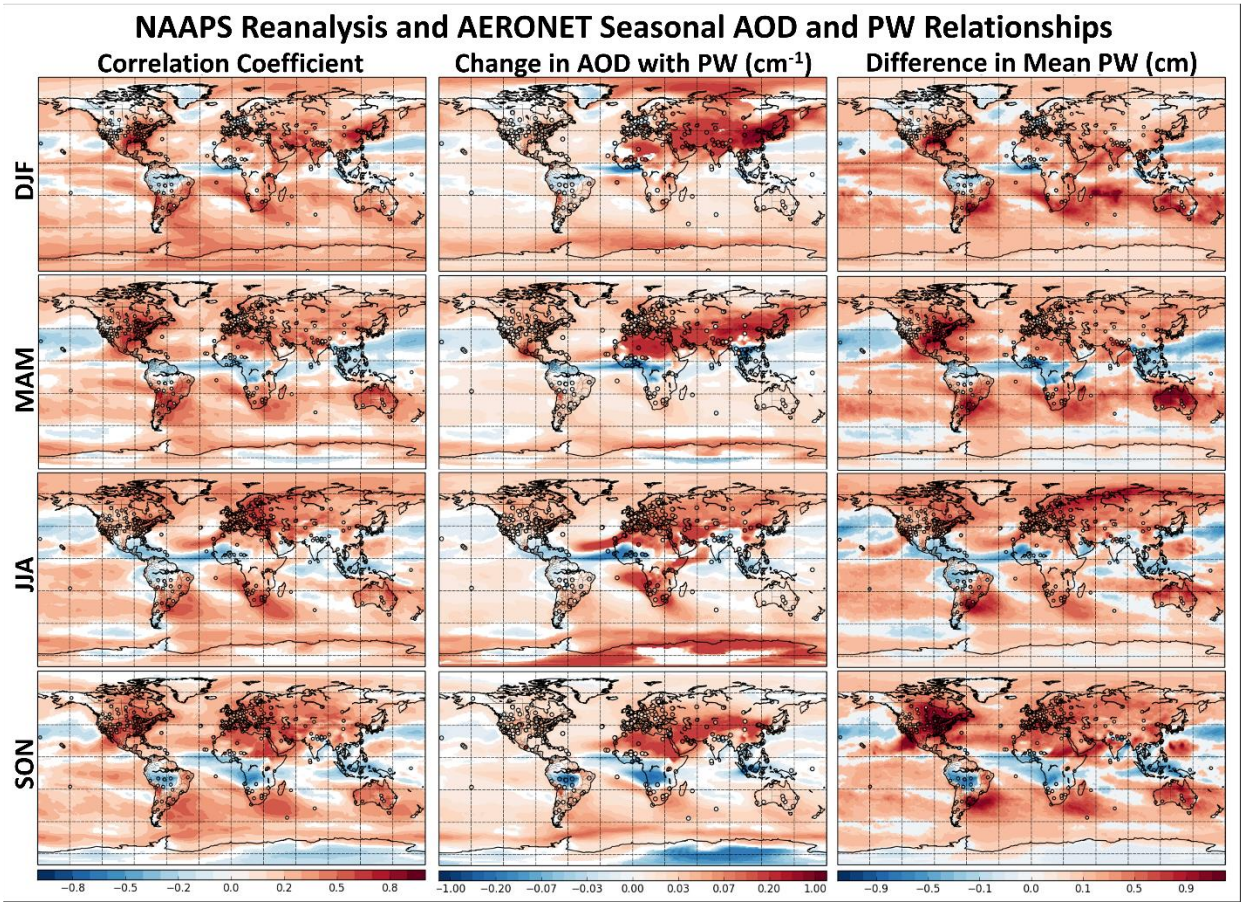

Figure 3. Seasonal AOD and PW relationships based on AERONET data (circles) and the NAAPS-RA (global map) shown as: 1) correlation coefficients between daily-averaged AOD and PW (non-zero values are statistically significant at the 95% level) 2) Theil-Sen regression slopes (change in AOD with PW) between daily-averaged AOD and PW in units of cm-1 at locations where the correlation is statistically significant and 3) the statistically significant difference in mean PW (cm) between the PW distribution associated with high AOD events (> 1 standard deviation above mean) and the PW distribution for all AOD values. Red regions indicate a positive relationship between AOD and PW (higher moisture conditions for higher AOD events) and blue regions indicate a negative relationship (dryer conditions for higher AOD events).

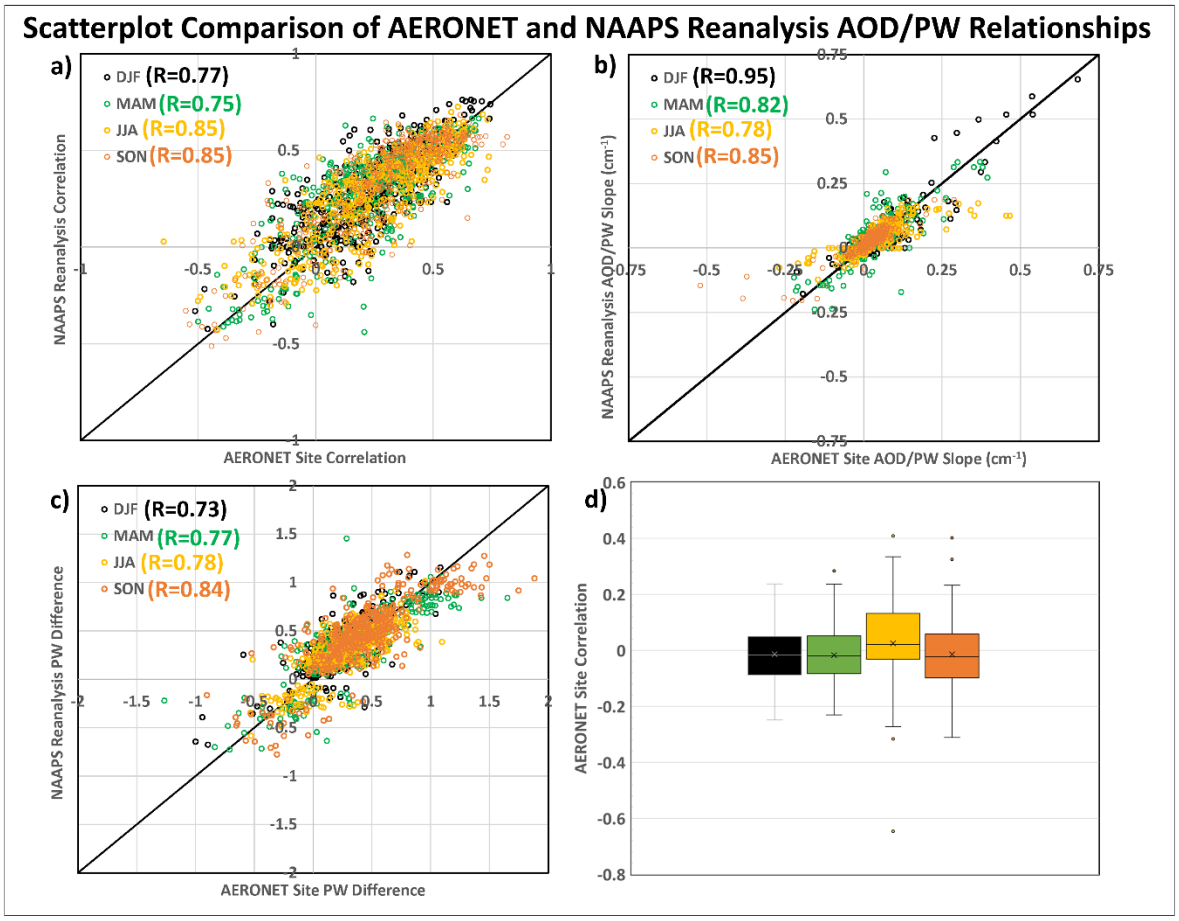

Figure 4. Scatterplot comparisons of the NAAPS-RA and AERONET: a) AOD and PW correlations at AERONET sites b) the change in AOD with PW (cm-1) at AERONET sites and c) the statistically significant difference in mean PW associated with high AOD events compared to the full PW distribution at AERONET sites. The comparisons are shown by season (DJF, MAM, SON, JJA) and correlations between the datasets are included. Additionally, the distribution of AERONET site correlations for which sign differences were found between NAAPS and AERONET calculated AOD/PW relationships are shown seasonally in d).

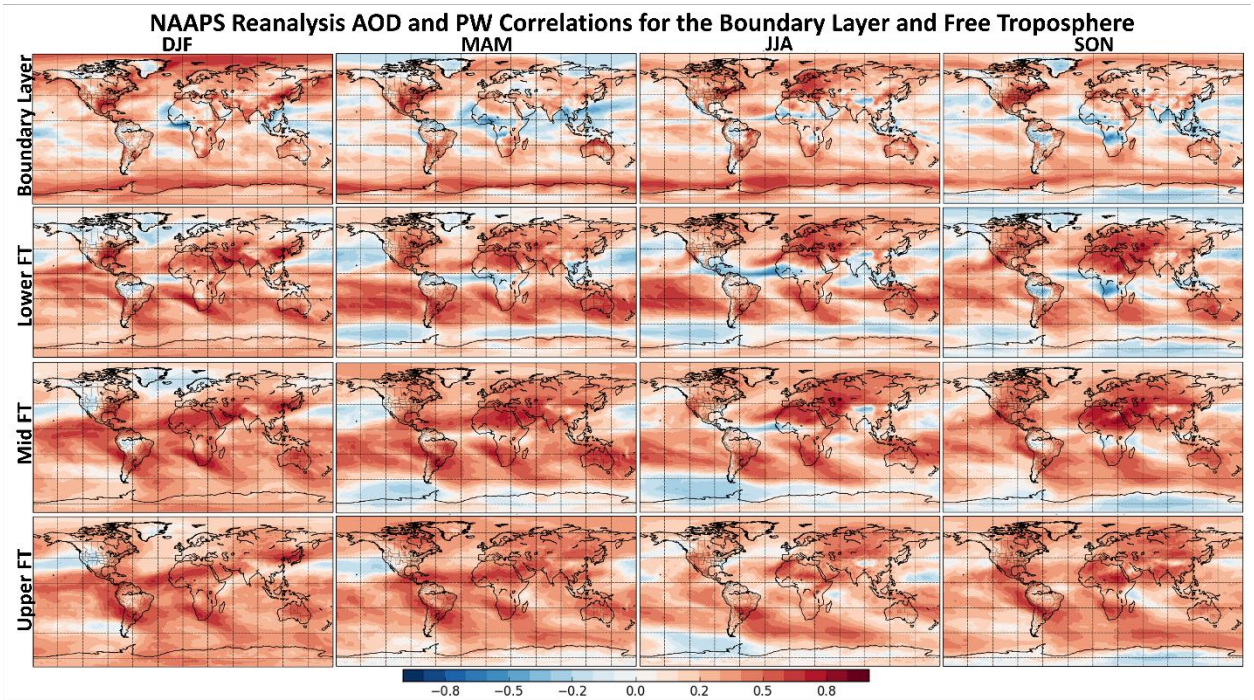

Figure 5. NAAPS-RA seasonal correlations (DJF, MAM, JJA, SON) between vertically-integrated total aerosol extinction and specific humidity in the boundary layer, lower free troposphere, mid free troposphere and upper free troposphere. Red values indicate a positive correlation and blue values indicate a negative correlation.

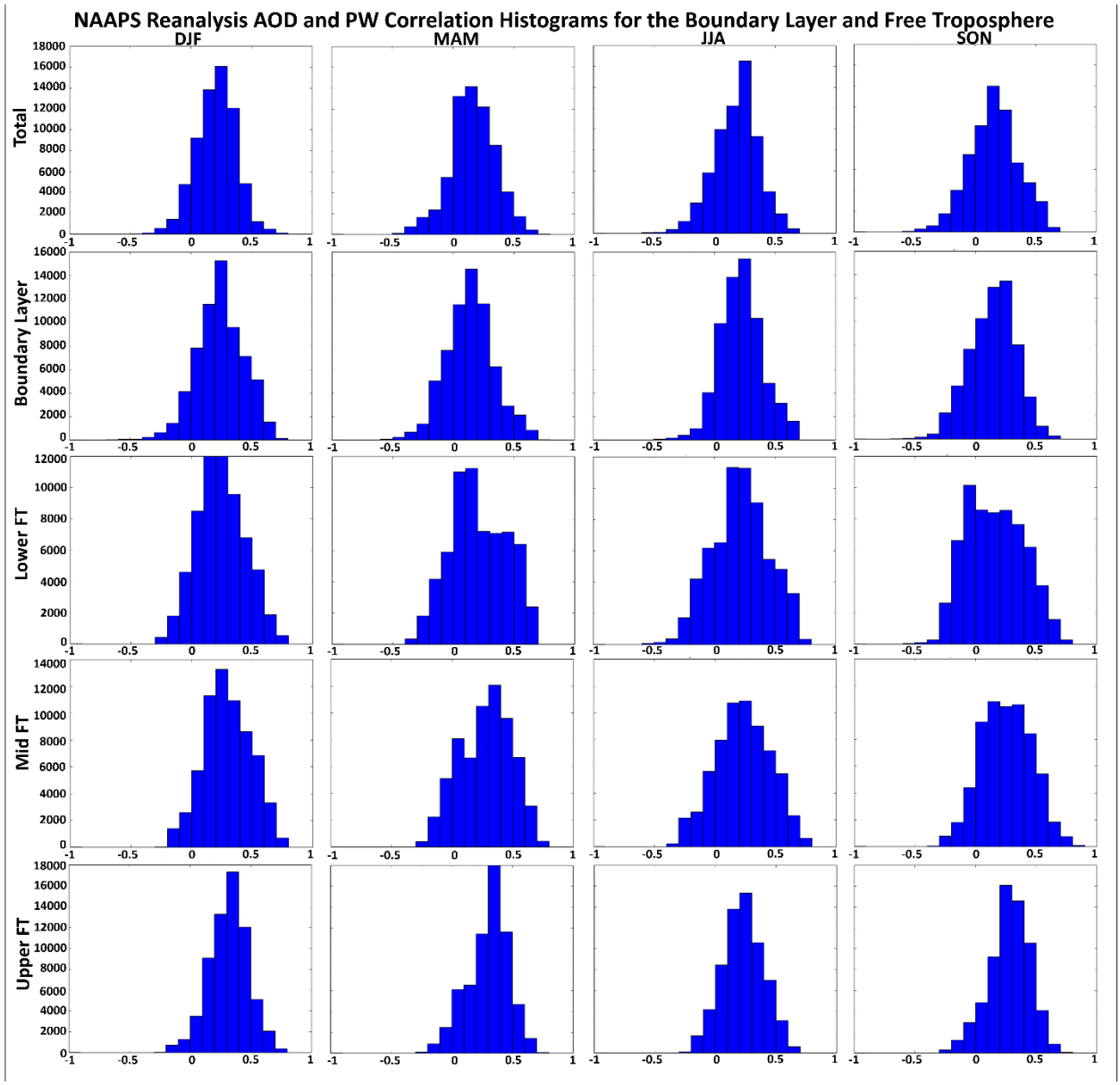

Figure 6. AOD and PW correlation histograms by season for the full integrated column (Total) and vertical components of the atmosphere (Boundary Layer, Lower/Mid/Upper Free Troposphere).

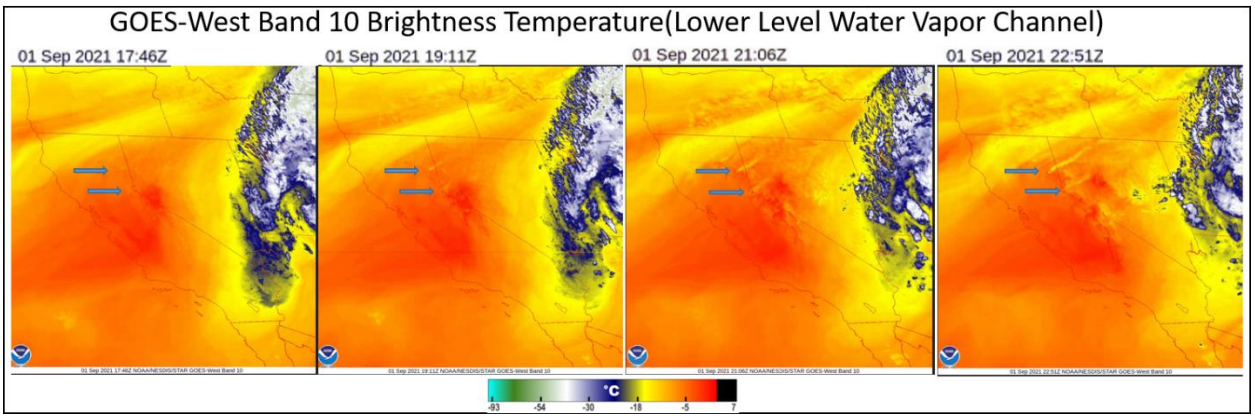

Figure 7. GOES-West 7.3um (Band 10) water vapor channel brightness temperature for a smoke event in California on September 1, 2021. The blue arrows point to the location of the California fires. As time progresses, the transport of the smoke can be seen with cooler brightness temperatures.

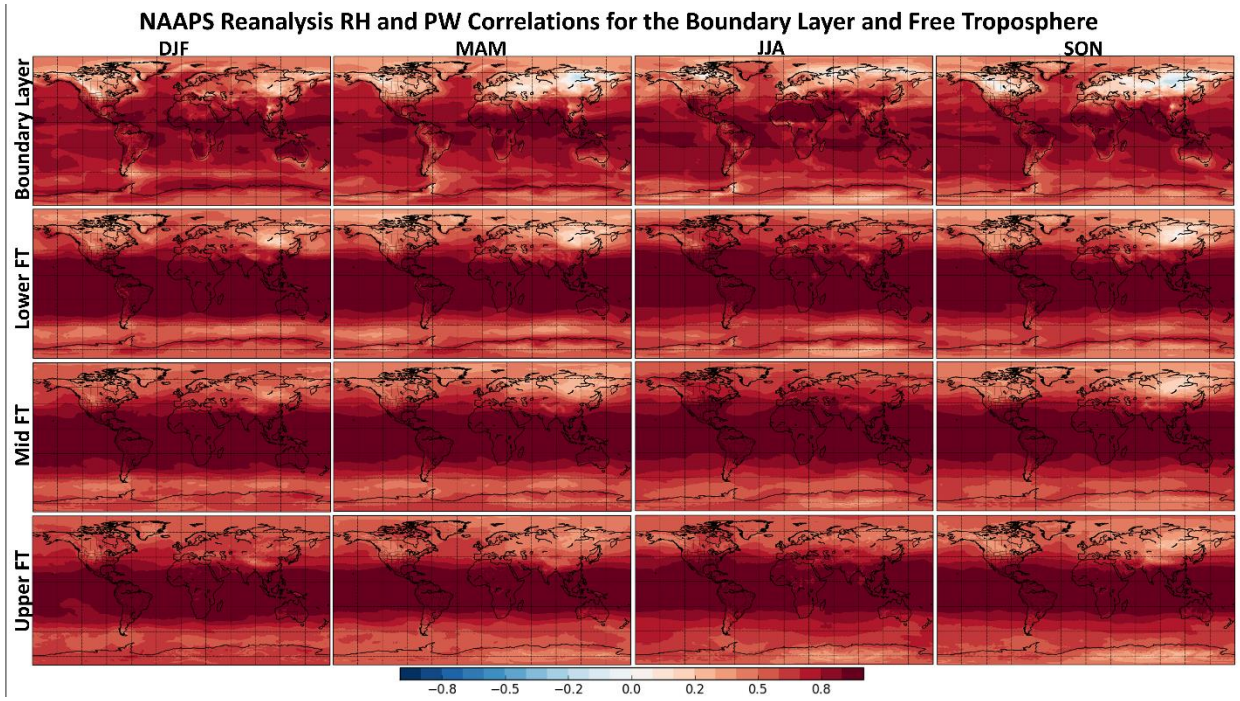

Figure 8. NAAPS-RA seasonal correlations (DJF, MAM, JJA, SON) between vertically-integrated relative humidity (integrated specific humidity/integrated saturation specific humidity) and specific humidity in the boundary layer, lower free troposphere, mid free troposphere and upper free troposphere.

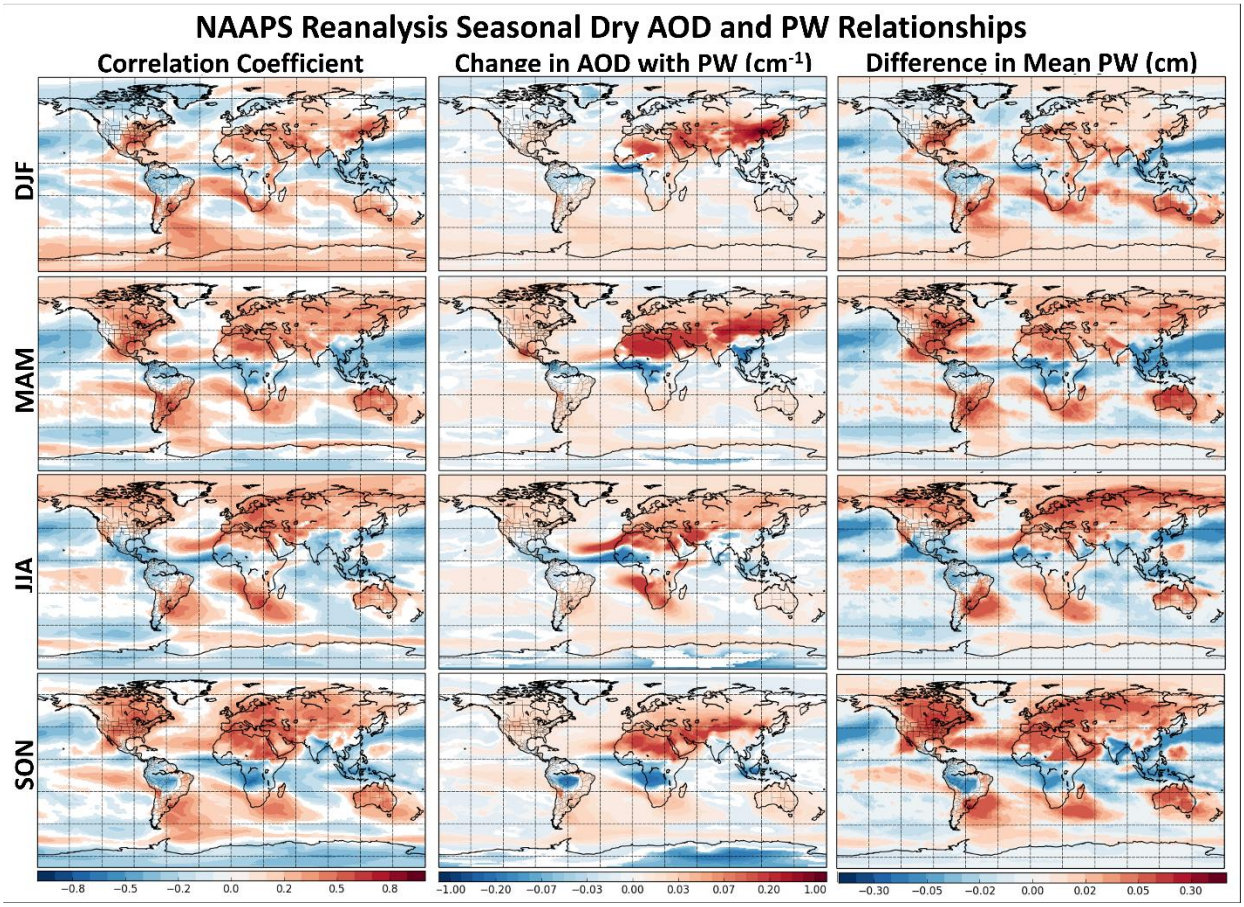

Figure 9. Seasonal dry AOD and PW relationships based on the NAAPS-RA shown as: 1)correlation coefficients between daily-averaged dry AOD and PW (non-zero values are statistically significant at the 95% level) 2) Theil-Sen regression slopes (change in AOD with PW) between daily-averaged dry AOD and PW in units of cm-1 at locations where the correlation is statistically significant and 3) the statistically significant difference in mean PW (cm) between the PW distribution associated with high dry AOD events (> 1 standard deviation above mean) and the PW distribution for all AOD values. Red regions indicate a positive relationship between dry AOD and PW and blue regions indicate a negative relationship.

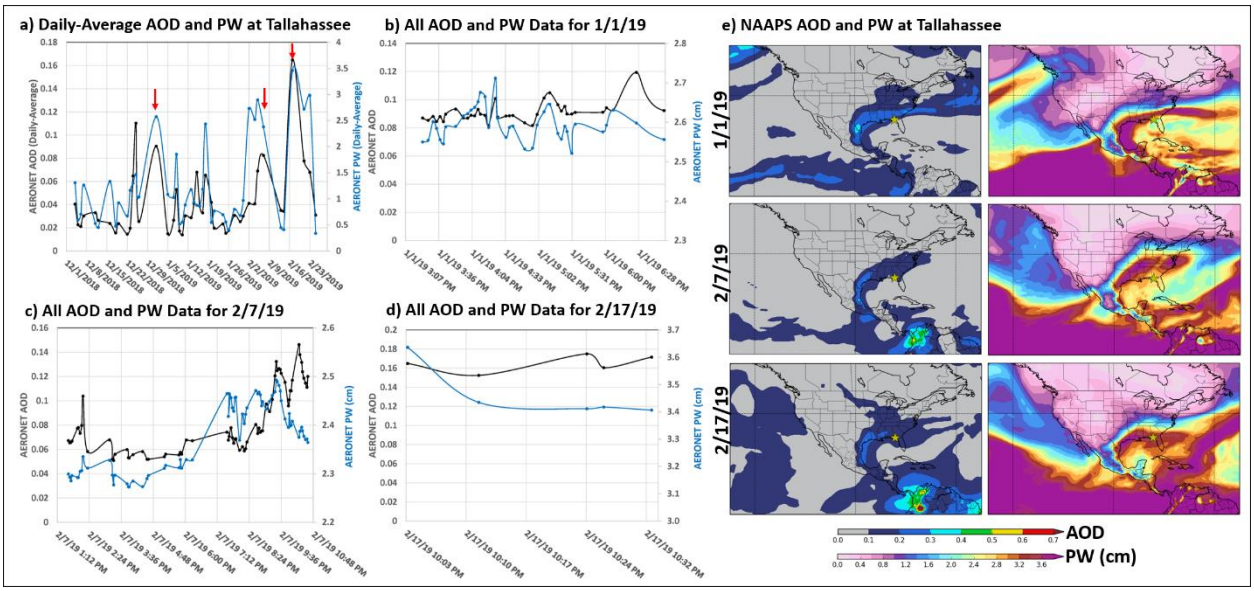

Figure 10. AOD and PW timeseries at the Tallahassee, Florida site in which strong positive correlations are observed during the DJF season. The daily-average AOD and PW timeseries are shown for the 2018-2019 DJF season with red arrows indicating select events for which joint peaks in AOD and PW are observed (a). Timeseries of AERONET data (non-averaged, all data) for dates identified with red arrows are shown in timeseries b-d. Additionally, NAAPS-RA AOD and PW (cm) fields are shown for the same dates with the AERONET site marked with a yellow star (e).

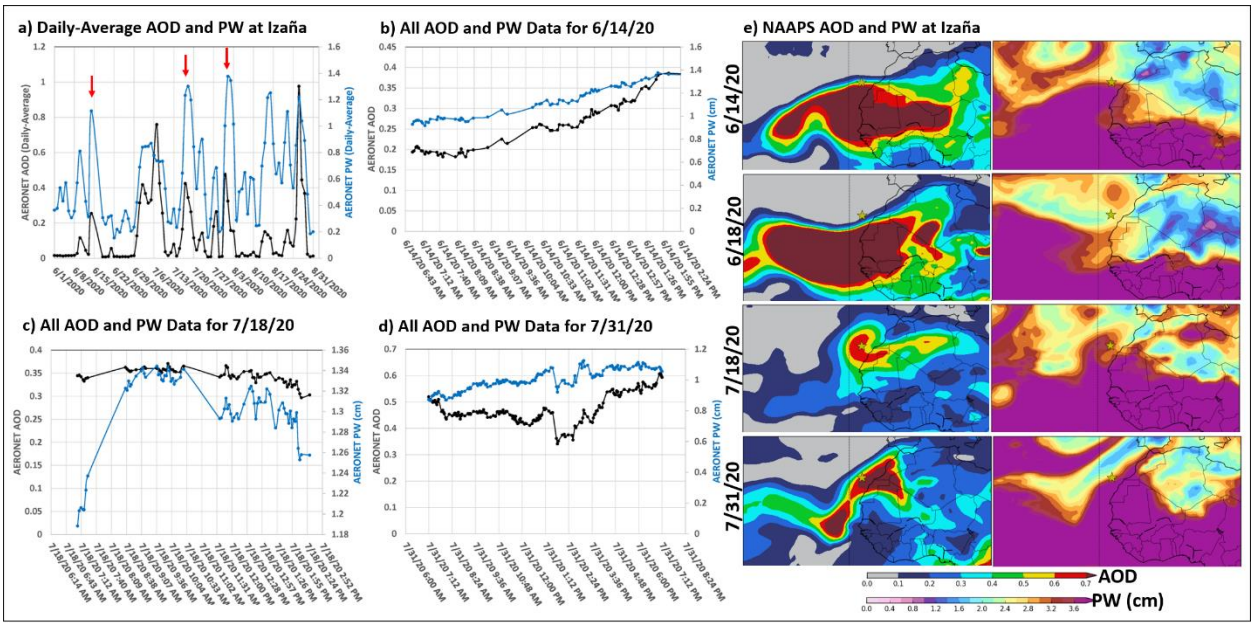

Figure 11. AOD and PW timeseries at the Izana, Canary Islands site in which strong positive correlations associated with dust are observed during the JJA season. The daily-average AOD and PW timeseries are shown for the 2020 JJA season with red arrows indicating select events for which joint peaks in AOD and PW are observed (a). Timeseries of AERONET data (non-averaged, all data) for dates identified with red arrows are shown in timeseries b-d. Additionally, NAAPS-RA AOD and PW (cm) fields are shown for the same dates with the AERONET site marked with a yellow star (e). The fields for 6/18/20 are also included which show the joint dip in AOD and PW in the (a) timeseries after the 6/14 event.

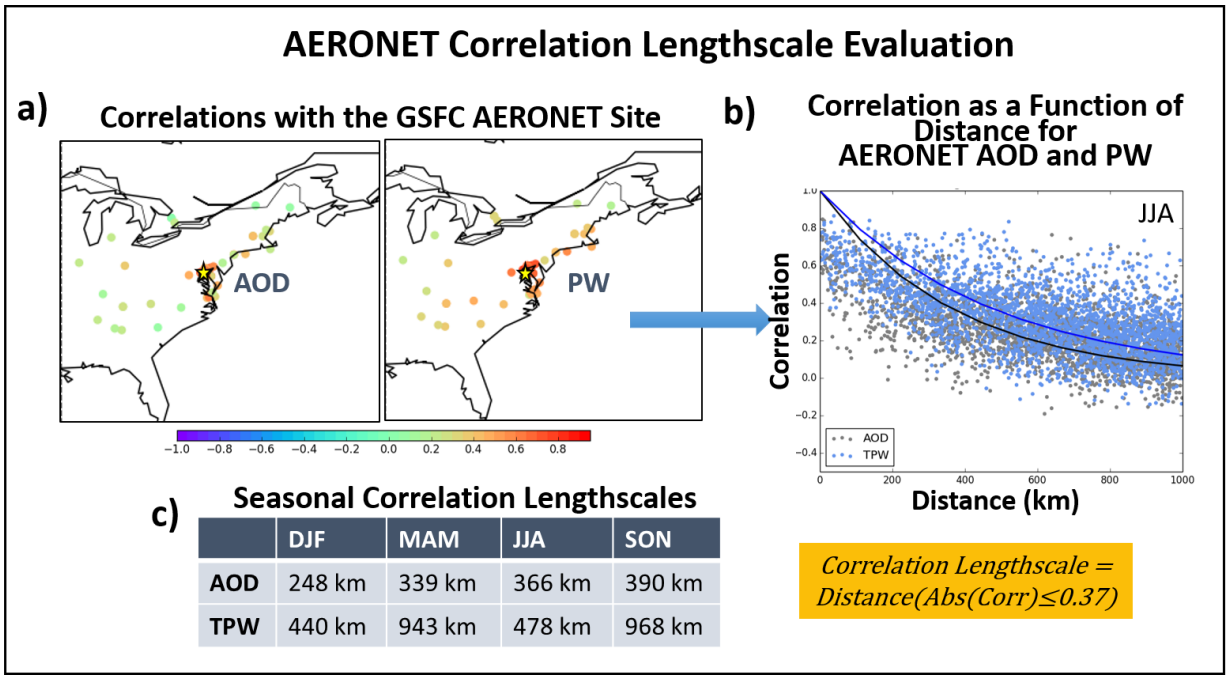

	DJF	MAM	JJA	SON
AOD	248 km	339 km	366 km	390 km
TPW	440 km	943 km	478 km	968 km

Figure 12. AERONET correlation lengthscale evaluation for AOD and PW in the Eastern United States. An example correlation calculation for the Goddard Space Flight Center (GSFC) site is shown in a). This analysis is conducted for all sites resulting in what is shown in b) with correlation as a function of distance. The correlation lengthscale is defined as when the correlation falls below 0.37 with the seasonal results for AOD and PW shown in c).

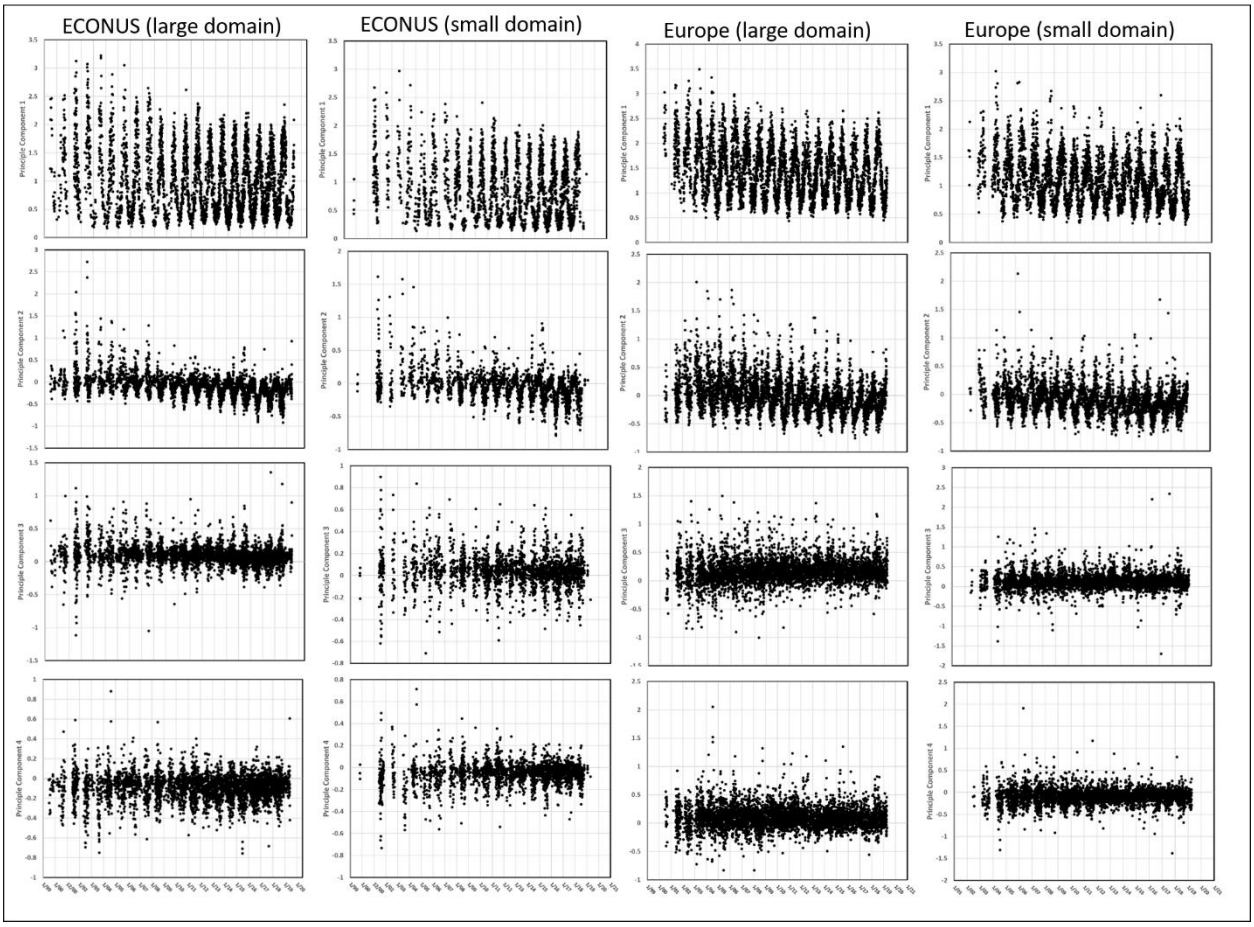

Figure 13. Principle component (1-4) from 1999 through 2021 for the Eastern Continental United States (ECONUS) and Europe domains with results shown for a larger and smaller domain for each region.

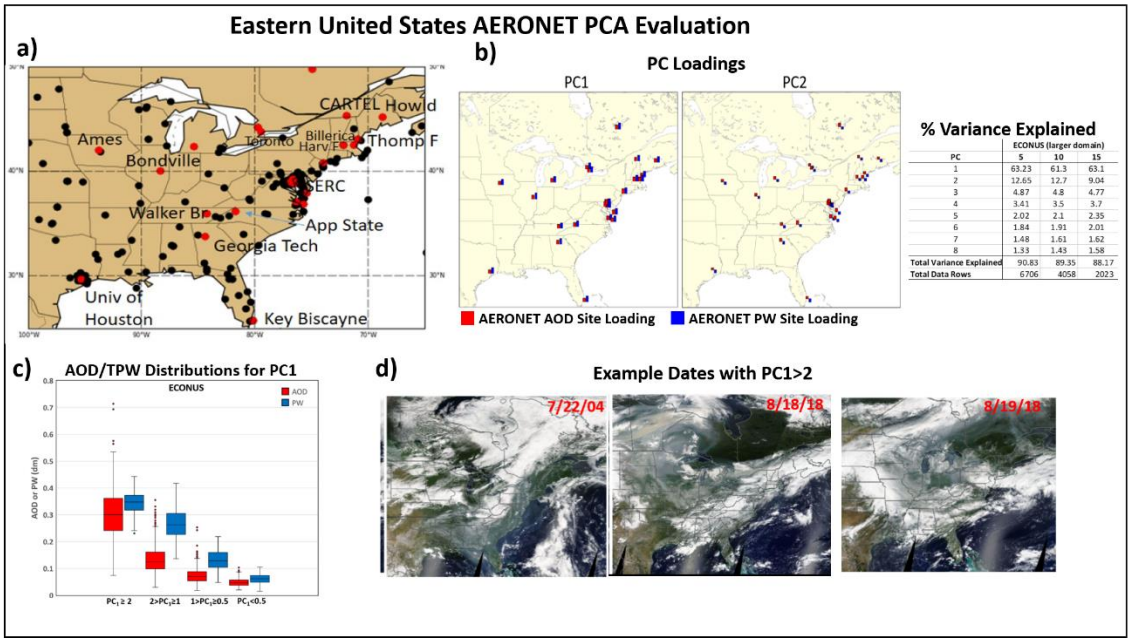

Figure 14. Results of the PCA analysis for the Eastern Continental United States (large domain) region. A map of all available AERONET sites (black, used for OK) and sites used in the PCA (red) is shown in a). A map of the loadings for the PCs is shown in b). The distribution of AOD and PW values associated with different PC1 ranges is shown in c) and some example true color images of events that had high PC1 values associated with them is shown in d).

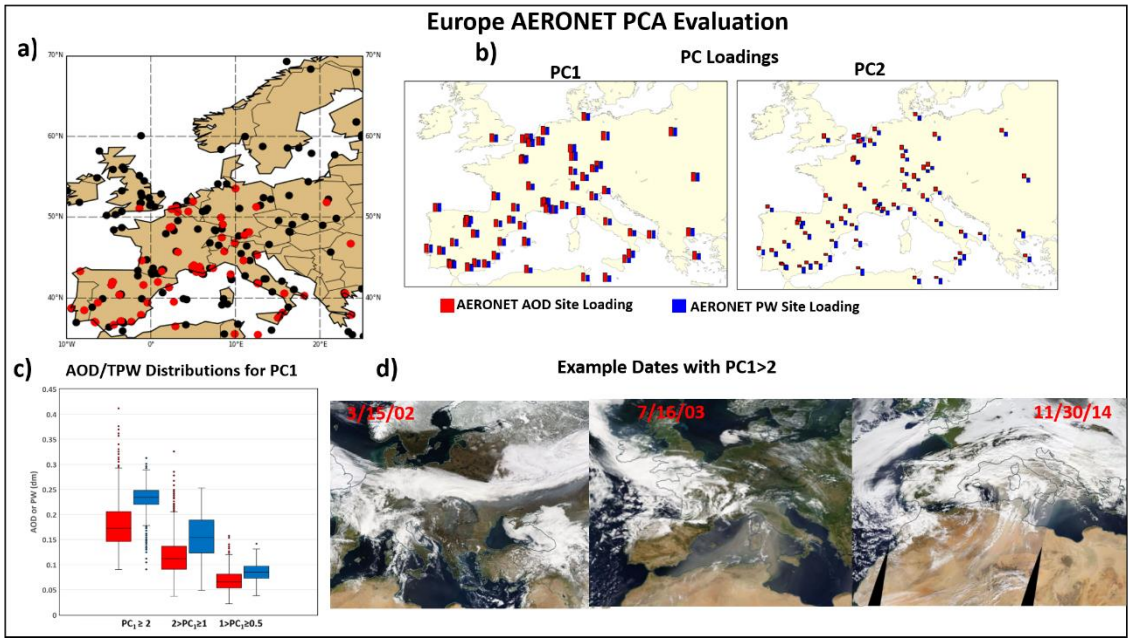

Figure 15. Results of the PCA analysis for the Europe (large domain) region. A map of all available AERONET sites (black, used for OK) and sites used in the PCA (red) is shown in a). A map of the loadings for the PCs is shown in b). The distribution of AOD and PW values associated with different PC1 ranges is shown in c) and some example true color images of events that had high PC1 values associated with them is shown in d).

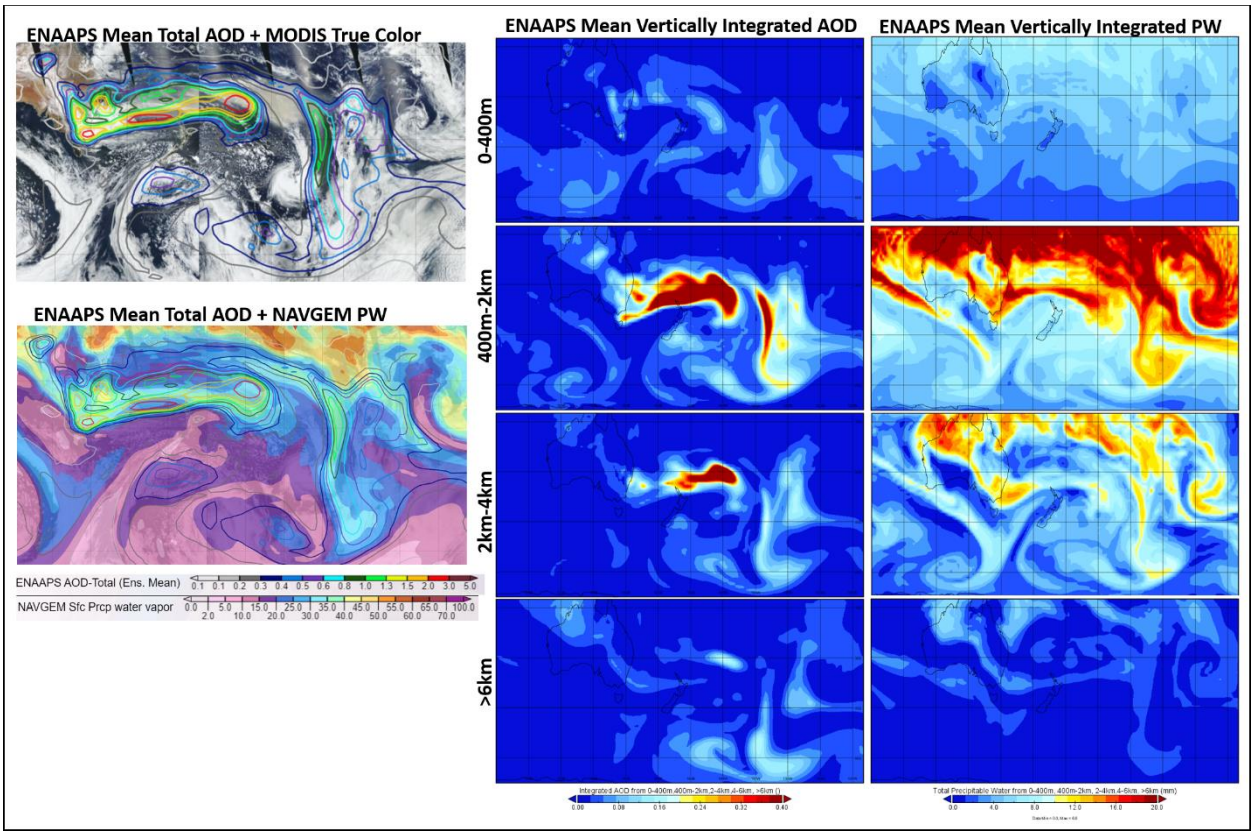

Figure 16. Evaluation of ENAAPS aerosol forecast on 1/6/2020 for extreme Australian wildfires. Results include the ENAAPS mean total AOD (unfilled contour) on a MODIS true color image where we can see locations where the model misses high AOD regions (upper left), the ENAAPS mean total AOD (unfilled contour) on NAVGEM PW fields (bottom left), ENAAPS mean AOD and PW integrated over 0-400m, 400m-2km, 2-4km, 4-6km, and greater than 6km. This shows where the modeled aerosol is predominantly located vertically in the atmosphere.

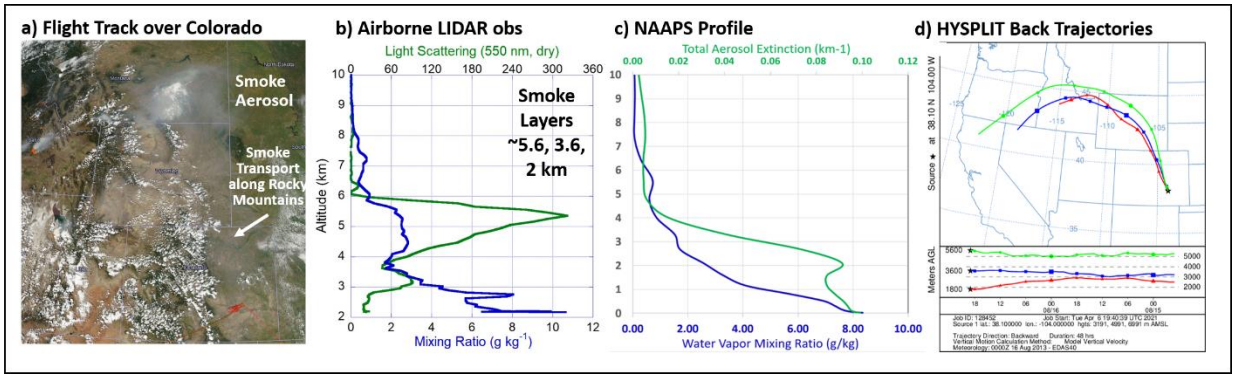

Figure 17. Evaluation of airborne and model data from the SEAC4RS field campaign in the United States. A true color image for 8/16/13 is shown with flight tracks (red lines) shown and MODIS fire detections (red dots) in a). Profiles of water vapor mixing ratio and light scattering are shown from the airborne lidar with smoke layers present at ~ 2, 3.6 and 5.6 km in b). NAAPS model profiles of water vapor mixing ratio and aerosol extinction are shown in c) and HYSPLIT back trajectories from the 3 aerosol layers in the LIDAR data is shown in d).

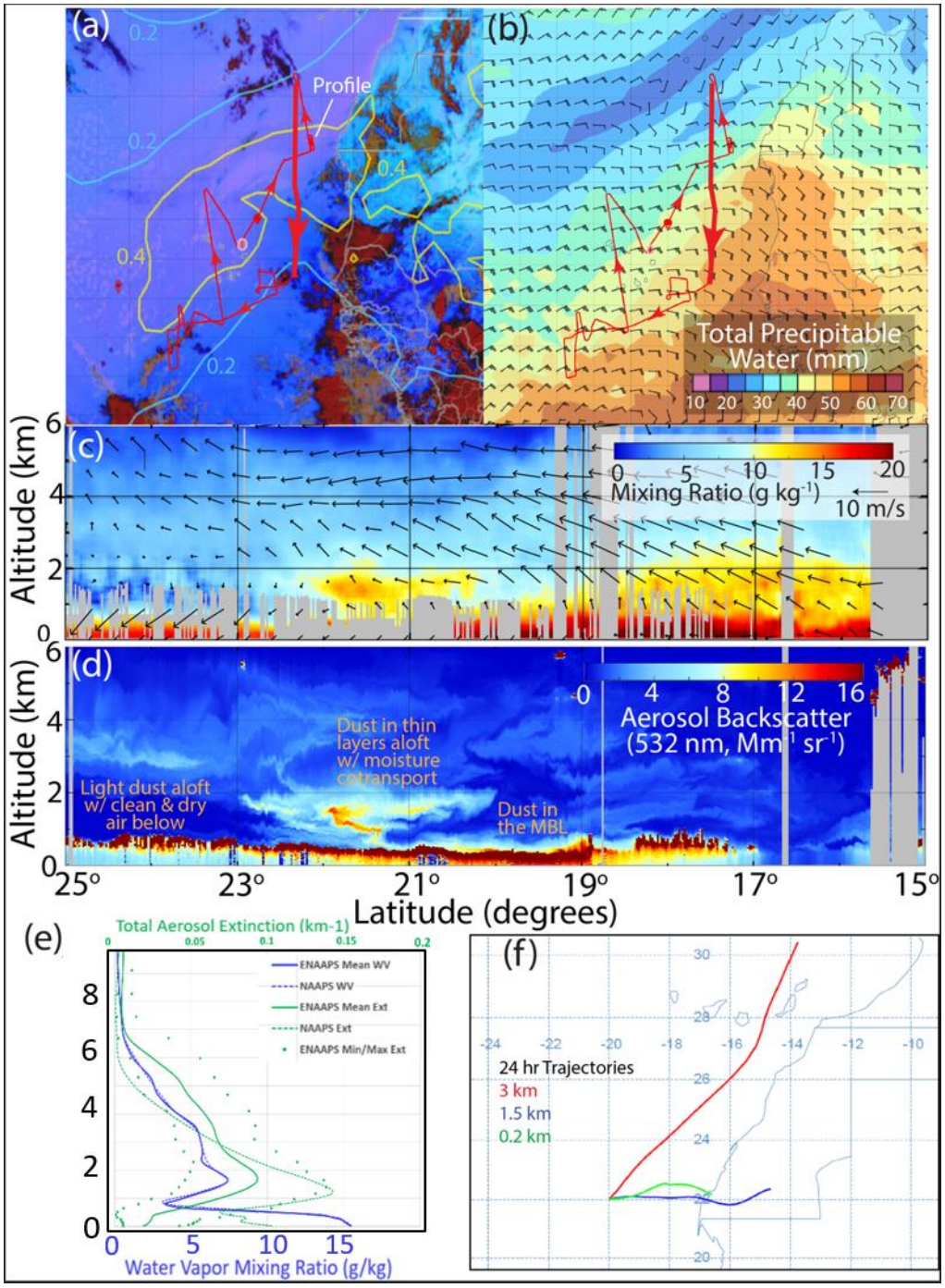

Figure 18. Evaluation of aircraft measurements, satellite data, and model output for a sampled dust event during CPEX on 9/9/22. Model output is shown at 22˚N, consistent with the dust aloft with moisture co-transport and the same point from which HYSPLIT back trajectories were run in (f).

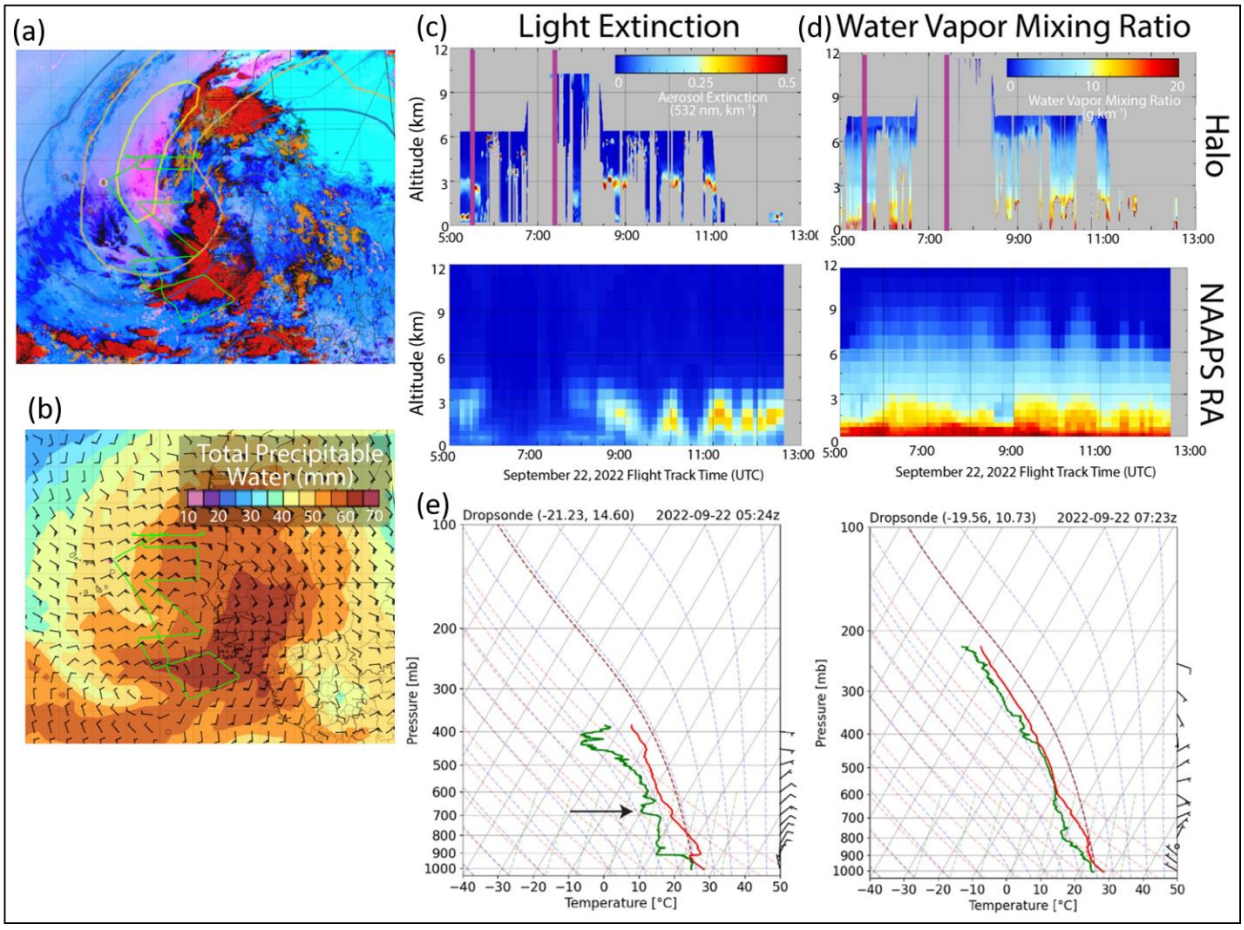

Figure 19. CPEX evaluation of a large dust event on September 22, 2022.

REFERENCES

Barreto, Á., Cuevas, E., García, R. D., Carrillo, J., Prospero, J. M., Ilić, L., Basart, S., Berjón, A. J., Marrero, C. L., Hernández, Y., Bustos, J. J., Ničković, S., and Yela, M.: Long-term characterization of the vertical structure of the Saharan Air Layer over the Canary Islands using lidar and radiosonde profiles: implications for radiative and cloud processes over the subtropical Atlantic Ocean, Atmos. Chem. Phys., 22, 739–763, https://doi.org/10.5194/acp-22-739-2022, 2022.

Charlson, R.J., S.E. Schwartz, J.M. Hales, R.D. Cess, J.A. Coakley, Jr., J.E. Hansen, and D.J. Hoffman: Climate forcing by anthropogenic aerosols. *Science*, 255, 423-430, doi:10.1126/science.255.5043.423, 1992.

De Tomasi, F., and Perrone, M. R.: Lidar measurements of tropospheric water vapor and aerosol profiles over southeastern Italy, J. Geophys. Res., 108, 4286, doi:10.1029/2002JD002781, 2003.

Eck, T. F., Holben, B. N., Reid, J. S., Xian, P.,Giles, D. M., Sinyuk, A., Smirnov, A., Schafer, J.S., Slutsker, I., Kim, J., Koo, J.-H., Choi, M., Kim, K.C., Sano, I., Arola, A., Sayer, A.M., Levy, R.C., Munchak, L.A., O'Neill, N.T., Lyapustin, A., Hsu, N.C., Randles, C.A., Da Silva, A.M., Buchard, V., Govindaraju, R.C., Hyer, E., Crawford, J.H., Wang, P., Xia, X.: Observations of the interaction and transport offine mode aerosols with cloud and/or fog in Northeast Asia from Aerosol Robotic Network and satellite remote sensing.Journal of GeophysicalResearch: Atmospheres,123, 5560–5587.https://doi.org/10.1029/2018JD028313, 2018.

Giles, D. M., Sinyuk, A., Sorokin, M. G., Schafer, J. S., Smirnov, A., Slutsker, I., Eck, T. F., Holben, B. N., Lewis, J. R., Campbell, J. R., Welton, E. J., Korkin, S. V., and Lyapustin, A. I.: Advancements in the Aerosol Robotic Network (AERONET) Version 3 database – automated near-real-time quality control algorithm with improved

cloud screening for Sun photometer aerosol optical depth (AOD) measurements, Atmos. Meas. Tech., 12, 169–209, https://doi.org/10.5194/amt-12-169-2019, 2019.

Gutleben, M., Groß, S., Wirth, M., Emde, C., & Mayer, B.: Impacts of water vapor on Saharan air layer radiative heating. Geophysical Research Letters, 46, 14854– 14862, https://doi.org/10.1029/2019GL085344, 2019.

Hänel, G.: The properties of atmospheric aerosol particles as functions of the relative humidity at thermo- dynamic equilibrium with the surrounding moist air. Adv. Geophys. 19, 73-18, https://doi.org/10.1016/S0065-2687(08)60142-9, 1976.

Hogan, T. F., Liu, M., Ridout, J. S., Peng, M. S., Whitcomb, T. R., Ruston, B. C., Reynolds, C. A., Eckermann S. D., Moskaitis, J. R., Baker, N. L., McCormack, J. P., Viner, K. C., McLay, J. G., Flatau, M. K., Xu, L., Chen, C., and Chang, S. W.: The Navy Global Environmental Model. Oceanography, Special Issue on Navy Operational Models, 27, No. 3. 2014.

Holben, B. N., Eck, T. F., Slutsker, I., Tanré, D., Buis, J. P., Setzer, A., Vermote, E., Reagan, J. A., Kaufman, Y. J., Nakajima, T., Lavenu, F., Jankowiak, I., & Smirnov, A.: AERONET - A federated instrument network and data archive for aerosol characterization. Remote Sensing of Environment, 66(1), 1-16, https://doi.org/10.1016/S0034-4257(98)00031-5, 1998.

Kablick, G. P., Allen, D. R., Fromm, M. D., and Nedoluha, G. E: Australian PyroCb Smoke Generates Synoptic-Scale Stratospheric Anticyclones. Geophys. Res. Lett. 47, Issue13, https://doi.org/10.1029/2020GL088101, 2020.

Karyampudi, V. M., Palm, S.P., Reagen, J.A., Fang, H., Grant, W.B, Hoff, R.M., Moulin, C., Pierce, H.F., Torres, O., Browell, E.V., and Melfi, S.H.: Validation of the Saharan dust plume conceptual model using Lidar, Meteosat, and ECMWF data, Bull. Am. Meteorol. Soc., 80, 1045 – 1074, https://doi.org/10.1175/1520-0477(1999), 1999.

Kleinman, L.I., and Daum, P.H.: Vertical distribution of aerosol particles, water vapor, and insoluble trace gases in convectively mixed air, J. Geophys. Res. Atmos.,96 (D1), 991-1005, https://doi.org/10.1029/90JD02117, 1991.

Kuciauskas, A. P., Xian, P., Hyer, E. J., Oyola, M. I., & Campbell, J. R.: Supporting Weather Forecasters in Predicting and Monitoring Saharan Air Layer Dust Events as They Impact the Greater Caribbean, Bulletin of the American Meteorological Society, 99(2), 259-268, https://doi.org/10.1175/BAMS-D-16-0212.1, 2018.

Liu, D., Zhao, T., Boiyo, R., Chen, S., Lu, Z., Wu, Y., Zhao, Y.: Vertical structures of dust aerosols over East Asia based on CALIPSO retrievals. Remote Sens., 11,701; doi:10.3390/rs11060701, 2019.

Livingston, J. M., Russell, P. B., Reid, J. S., Redemann, J., Schmidt, B., Allen, D. A., Torres, O., Levy, R. C., Remer, L. A., Holben, B. N.m Smirnov, A., Dubovik, O., Welton, E. J., Campbell, J. R., Wang, J., Christopher, S. A.: Airborne Sun photometer measurements of aerosol optical depth and columnar water vapor during the Puerto Rico Dust Experiment and comparison with land, aircraft, and satellite measurements, J. Geophys. Res., 108, 8588, doi:10.1029/2002JD002520, D19, 2003.

Lynch, P., Reid, J. S., Westphal, D. L., Zhang, J., Hogan, T. F., Hyer, E. J., Curtis, C. A., Hegg, D. A., Shi, Y., Campbell, J. R., Rubin, J. I., Sessions, W. R., Turk, F. J., and Walker, A. L.: An 11-year global gridded aerosol optical thickness reanalysis (v1.0) for atmospheric and climate sciences, Geosci. Model Dev., 9, 1489–1522, https://doi.org/10.5194/gmd-9-1489-2016, 2016.

Nehrir, A., Notari, A., Harper, D., Fitzpatrick, F., Collins, J., Kooi, S., Antill, C., Hare, R., Barton-Grimley, R. A., Hair, J., Ferrare, R., Hostetler, C., and Welch, W.: The High Altitude Lidar Observatory (HALO): A multi-function lidar and technology test-bed for airborne and space-based measurements of water vapor and methane, NASA Earth Science Technology Office, http://www.estotechnology.us/techportfolio/pdf/additionalInfo/1914_Nehrir/Nehrir_ESTF2018_A1P2., 2018.

Peterson, D.A., Fromm, M.D., McRae, R.H.D.: Australia's Black Summer pyrocumulonimbus super outbreak reveals potential for increasingly extreme stratospheric smoke events. Clim Atmos Sci 4, 38, https://doi.org/10.1038/s41612-021-00192-9, 2021.

Reid, J. S., Kinney, J. E., Westphal, D. L., Holben, B. N., Welton, E. J., Tsay, S.-C., Christopher, S. A., Eleuterio, D. P., Campbell, J. R., Jonsson, H. H., Livingston, J. M., Maring, H. B., Meier, M., Pilewskie, P., Reid, E. A., . Russell, P. B., Savoie, D., Smironov, A., and D. Tanré D.: Analysis of measurements of Saharan dust by airborne

and ground-based remote sensing methods during the Puerto Rico Dust Experiment (PRIDE), J. Geophys. Res., 108, 8586, doi:10.1029/2002JD002493, D19, 2003.

Reid, J. S., Piketh, S., Burger, R., Ross, K., Jensen, T., Bruintjes, R., Walker, A., Al Mandoos, A., Miller, S., Hsu, C., Kuciauskas, A., and Westphal. , D. L.: An overview of UAE2 flight operations: Observations of summertime atmospheric thermodynamic and aerosol profiles of the southern Arabian Gulf, J. Geophys. Res., 113, D14213, doi:10.1029/2007JD009435, 2008.

Reid, J. S., Posselt, D. J., Kaku, K., Holz, R. A., Chen, G., Eloranta, E. W., Kuehn, R. E., Woods, S., Zhang, J., Anderson, B., Bui, T. P., Diskin, G. S., Minnis, P., Newchurch, M. J., Tanelli, S., Trepte, C. R., Thornhill, K. L., and Ziemba, L. D.: Observations and hypotheses related to low to middle free tropospheric aerosol, water vapor and altocumulus cloud layers within convective weather regimes: a SEAC4RS case study, Atmos. Chem. Phys., 19, 11413–11442, https://doi.org/10.5194/acp-19-11413-2019, 2019.

Reid, J.S., et al. : The coupling between tropical meteorology, aerosol lifecycle, convection, and radiation, during the Cloud, Aerosol and Monsoon Processes Philippines Experiment (CAMP2Ex). *Bull. Amer. Meteorol. Soc.*, 104, no. 6, E1179-E1205, doi:10.1175/BAMS-D-21-0285.1, 2023.

Resquin, M.D., Santagata, D., Gallardo, L., Gomez, D., Rossler, C., Dawidowski, L.: Local and remote black carbon sources in the Metropolitan Area of Buenos Aires. Atmospheric Environment. Volume 182, Pages 105-114, https://doi.org/10.1016/j.atmosenv.2018.03.018, 2018.

Rubin, J. I., Reid, J. S., Hansen, J. A., Anderson, J. L., Collins, N., Hoar, T. J., Hogan, T., Lynch, P., McLay, J., Reynolds, C. A., Sessions, W. R., Westphal, D. L., and Zhang, J.: Development of the Ensemble Navy Aerosol Analysis Prediction System (ENAAPS) and its application of the Data Assimilation Research Testbed (DART) in support of aerosol forecasting, Atmos. Chem. Phys., 16, 3927–3951, https://doi.org/10.5194/acp-16-3927-2016, 2016.

Rubin, J.I., Reid, J.S., Xian, P., Selman, C.M., and Eck, T.F.: A Global Evaluation of Daily to Seasonal Aerosol and Water Vapor Relationships Using a Combination of AERONET and NAAPS Reanalysis Data. Atmos. Chem. Phys., 23, 4059-4090, https://doi.org/10.5194/acp-23-4059-2023, 2023.

Ryder, C. L.: Radiative effects of increased water vapor in the upper Saharan Air Layer associated with enhanced dustiness. Journal of Geophysical Research: Atmospheres, 126, e2021JD034696, https://doi.org/10.1029/2021JD034696, 2021.

Sessions, W. R., Reid, J. S., Benedetti, A., Colarco, P. R., da Silva, A., Lu, S., Sekiyama, T., Tanaka, T. Y., Baldasano, J. M., Basart, S., Brooks, M. E., Eck, T. F., Iredell, M., Hansen, J. A., Jorba, O. C., Juang, H.-M. H., Lynch, P., Morcrette, J.-J., Moorthi, S., Mulcahy, J., Pradhan, Y., Razinger, M., Sampson, C. B., Wang, J., and Westphal, D. L.: Development towards a global operational aerosol consensus: basic climatological characteristics of the International Cooperative for Aerosol Prediction Multi-Model Ensemble (ICAP-MME), Atmos. Chem. Phys., 15, 335–362, doi:10.5194/acp-15-335-2015, 2015.

Späth, F., Behrendt, A., Muppa, S. K., Metzendorf, S., Riede, A., and Wulfmeyer, V.: 3-D water vapor field in the atmospheric boundary layer observed with scanning differential absorption lidar, Atmos. Meas. Tech., 9, 1701–1720, https://doi.org/10.5194/amt-9-1701-2016, 2016.

Stull, R. B. and Eloranta, E. W.: Boundary Layer Experiment 1983, Bull. Amer. Meteorol. Soc., 65, 450–456, DOI: 10.1175/1520-0477(1984)065<0450:BLE>2.0.CO;2, 1984.

Su, H., Jiang, J.H., Liu, X., Penner, J.E., Read, W.G., Massie, S., Schoeberl, M.R., Colarco, P., Livesey, N.J., and Santee, M.L.: Observed increase of TTL temperature and water vapor in polluted clouds over Asia, Journal of Climate, 24(11), 2728-2736, https://doi.org/10.1175/2010JCLI3749.1, 2011.

Toon, O. B.: Planning, implementation, and scientific goals of the Studies of Emissions and Atmospheric Composition, Clouds and Climate Coupling by Regional Surveys (SEAC4RS) field mission, J. Geophys. Res. Atmos., 121, 4967–5009, doi:10.1002/2015JD024297, 2016.

Turner D.D., Ferrare, R.A., Heilman Brasseur, L.A., Feltz, W.F., and Tooman, T.P.: Automated Retrievals of Water Vapor and Aerosol Profiles from an Operational Raman Lidar. J. Atmos. Oceanic Tech, 19, 37-50, DOI:10.1175/1520-0426(2002), 2002.

Wimmers, A. J., C. S. Velden: Seamless Advective Blending of Total Precipitable Water Retrievals from Polar-Orbiting Satellites. J. Appl. Meteor. Climatol., 50, 1024-1036. doi: http://dx.doi.org/10.1175/2010JAMC2589.1, 2011.

Winker, D. M. et al. The CALIPSO Mission A Global 3D View of Aerosols and Clouds. Bull. Am. Meteorol. Soc. 91, 1211–1229, 2010.

Xian, P., Reid, J., Hyer, E., Sampson, C. Rubin, J., Ades, M., Asencio, N., Basart, S., Benedetti, A., Bhattacharjee, P.S., Brooks, M.E., Colarco, P.R., da Silva, A.M., Eck, T.F., Guth, J., Jorba, O., Kouznetsov, R., Kipling, Z., Sofiev, M., Perez Garcia-Pando, C., Pradhan, Y., Tanaka, T., Wang, J., Westphal, D.L., Yumimoto, K., and Zhang, J.: Current state of the global operational aerosol multi-model ensemble: An update from the International Cooperative for Aerosol Prediction (ICAP). Q.J.R. Meteorol. Soc. 145 (Suppl. 1): 176-209, DOI: 10.1002/qj.3497, 2019.